frontiers | Frontiers in Earth Science

ORIGINAL RESEARCH
published: 25 April 2022
doi: 10.3389/feart.2022.838867

Seasonal River Chemistry and Lithium Isotopes in the Min Jiang at Eastern Tibetan Plateau: Roles of Silicate Weathering and Hydrology

Baiyang Liu-Lu[1,2], Zhangdong Jin[1,3], Long-Fei Gou[1,4], Fei Zhang[1,4], Mao-Yong He[1,4] and Yang Xu[1,2]*

[1]SKLLQG, Institute of Earth Environment, Chinese Academy of Sciences, Xi'an, China, [2]University of Chinese Academy of Sciences, Beijing, China, [3]Institute of Global Environmental Change, Xi'an Jiaotong University, Xi'an, China, [4]School of Land Engineering, Chang'an University, Xi'an, China

Riverine lithium (Li) isotopes have been considered as a robust tracer for silicate weathering, but processes controlling riverine δ^7Li ratios remain controversial. To address the impacts of weathering and hydrology on riverine δ^7Li, the seasonal variation of water chemistry in the Min Jiang at the eastern Tibetan Plateau was investigated over December of 2009 to the end of 2010. The results showed distinct seasonal variations in ionic chemistry and δ^7Li. Increased river discharge in the monsoon season diluted dissolved ions, and monsoonal hydrological changes caused frequent δ^7Li fluctuations. High discharge caused by monsoonal rainfall reduced Li isotope fractionation by shortened rock–fluid interaction time, resulting in lower δ^7Li, whereas the input of high δ^7Li groundwater and landslide seepage elevated riverine δ^7Li, together with lengthened rock–fluid interaction time in less rain intervals. Based on the high-resolution sampling strategy and dataset over one hydrological year, this study highlights that changes of hydrological conditions can have a significant impact on weathering processes and water sources, and therefore on riverine δ^7Li variation.

Keywords: lithium isotopes, seasonality, hydrological change, silicate weathering, eastern Tibetan Plateau

OPEN ACCESS

Edited by:
Philippe Claeys,
Vrije Universiteit Brussel, Belgium

Reviewed by:
Santosh Kumar Rai,
Wadia Institute of Himalayan Geology, India
Sambuddha Misra,
Indian Institute of Science (IISc), India

****Correspondence:***
Zhangdong Jin
zhdjin@ieecas.cn

Specialty section:
This article was submitted to Geochemistry, a section of the journal Frontiers in Earth Science

Received: *18 December 2021*
Accepted: *16 March 2022*
Published: *25 April 2022*

Citation:
Liu-Lu B, Jin Z, Gou L-F, Zhang F, He M-Y and Xu Y (2022) Seasonal River Chemistry and Lithium Isotopes in the Min Jiang at Eastern Tibetan Plateau: Roles of Silicate Weathering and Hydrology. Front. Earth Sci. 10:838867. doi: 10.3389/feart.2022.838867

1 INTRODUCTION

Silicate weathering is thought to be a major sink of atmospheric CO_2, which regulates the carbon cycle and climate on geological time scales (e.g., Walker et al., 1981; Bickle et al., 2015; Penman et al., 2020); thus, it is in turn an important control on global climate. It has been argued that tectonic uplift and exposure of fresh rocks has a strong influence on the weathering rate (Edmond et al., 1995). The uplift of the Himalayas and the Tibetan Plateau had strengthened silicate weathering and atmospheric CO_2 consumption as a proposed trigger of global cooling since ~50 Ma (e.g., Raymo and Ruddiman, 1992; Clift et al., 2008). Since materials in rivers have been used to trace weathering, that is, particulate sediments corresponding to the physical denudation rate and dissolved loads to the chemical weathering rate, respectively (Li and Zhang, 2002), the rivers draining the southern Himalayas and the eastern Tibetan Plateau are widely explored on the relationship between the tectonics and climate with weathering rates (e.g., Qin et al., 2000; Bickle et al., 2005; Wu et al., 2011; Bickle et al., 2015). For example, recent studies have shown that in the Himalayas and Qinghai, from where main Chinese rivers originate, the long-term CO_2 consumption

by silicate weathering occupies 3.8% of global silicate weathering (Wu et al., 2008), implying the role of the tectonics in enhancing silicate weathering. Similarly, Bickle et al. (2015) demonstrated that Himalayan rivers are dominated by silicate inputs, up to 60% riverine Sr in the catchment on the High Himalayan Crystalline Series from silicates, after they reviewed geochemical analyses of river waters from the headwaters and their tributaries of the Himalayan rivers. More recently, seismically enhanced ionic fluxes after the 2008 Wenchuan earthquake resulted in a 4.3 ± 0.4 time increase in CO_2 consumption flux *via* silicate-derived alkalinity and a 0.000644 ± 0.000146 increase in $^{87}Sr/^{86}Sr$ isotopic ratios (Jin et al., 2016). At the millennial scale, silicate weathering was mainly related with runoff and physical erosion, while temperature played a secondary role (Dosseto et al., 2015). However, the relationships among silicate weathering, the carbon cycle, and climate at various time scales remain elusive. One of the key reasons is the lack of a robust tracer for silicate weathering.

So far, a number of isotopic tracers have been served for evaluating the silicate weathering rate and intensity, such as Sr, Mg, Si, and Os isotopes. However, none of them would be able to trace silicate weathering reliably, owing to the effects of other processes and/or unconstrained sources, such as biological processes for Mg and Si isotopes (Li et al., 2014; Mavromatis et al., 2016; Pogge von Strandmann et al., 2016), meta-carbonate-sourced radiogenic Sr (Edmond, 1992; Galy and France-Lanord, 1999; Bickle et al., 2005; Beck et al., 2013), and black shale-derived Os (Ravizza and Esser, 1993). Lithium (Li) is one of the most promising tracers for tracing silicate weathering. This is due to the fact that Li is hosted broadly in silicates, with significant fractionation during weathering (Huh et al., 1998; Huh et al., 2001). Li is soluble, with two stable isotopes (^6Li and ^7Li) that fractionate during low-temperature rock–fluid exchange reactions. Meanwhile, Li isotope variations are not significantly affected by biological processes (Lemarchand et al., 2010; Pogge von Strandmann et al., 2016). Thus, Li isotopes can record weathering and transportation information.

Due to the analytical technique development, research on Li isotope tracing silicate weathering has been blossoming in the last decade. Previous studies have mainly focused on the spatial variation of the riverine dissolved δ^7Li, factors that control riverine Li isotopic fractionation, and how to use riverine δ^7Li as a tracer of silicate weathering at various scales (Huh et al., 1998; Huh et al., 2001; Pogge von Strandmann et al., 2006; Vigier et al., 2008; Liu and Rudnick, 2011; Dellinger et al., 2014; Wang et al., 2015). However, the dominant processes controlling riverine δ^7Li ratios remain debatable (Misra and Froelich, 2012; Dellinger et al., 2015). To address this issue, time–series change of riverine δ^7Li ratios may provide helpful clues, because its sources and end-members can be well constrained or easily defined. Researchers found that there was a ~10% difference of δ^7Li at the same site in different seasons, and δ^7Li of samples showed seasonal variations (Kısakürek et al., 2005; Liu et al., 2015), but the resolution of time–series of previous studies was not high enough to decipher the role of climate (Gou et al., 2019). In addition, there were only

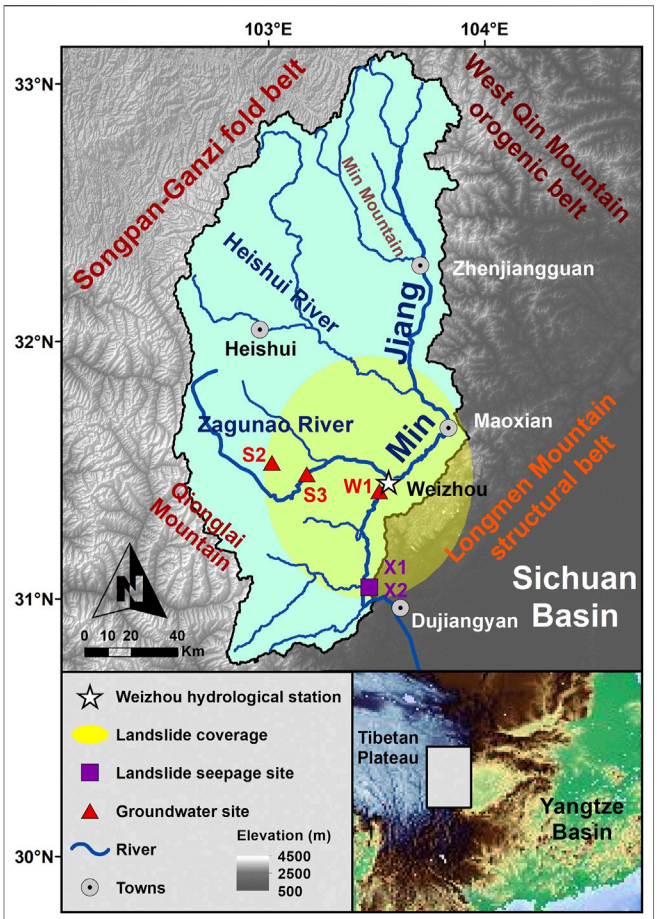

FIGURE 1 | Map of the Min Jiang catchment, including sampling sites of river water at the Weizhou hydrological station, groundwater, and landslide seepage.

a few studies that mentioned about the hydrological impacts on riverine δ^7Li (e.g., Lemarchand et al., 2010; Fries et al., 2019; Xu et al., 2021): how the hydrology (such as monsoon rain and groundwater) affecting riverine Li isotope behaviors is poorly constrained. Therefore, we set a high-resolution time–series research in order to explore the weathering processes in detail by seasonal riverine δ^7Li variation at the eastern Tibetan Plateau.

The earth surface processes on the Tibetan Plateau is sensitive to climate, and climate regulation by silicate weathering is strongest at such high elevations (West et al., 2002; Maher and Chamberlain, 2014; Caves et al., 2016; Ma et al., 2020). The Min Jiang is one of the primary tributaries of the Yangtze River, draining the eastern edge of the Tibetan Plateau (**Figure 1**). As a tectonically active and fast-eroding region, the weathering within the Min Jiang catchment would be significantly influenced by climate and hydrology, making it as an ideal setting for exploring the controlling factors of riverine δ^7Li ratios and its relationship with silicate weathering. In this study, we investigated water chemistry and Li isotope compositions of river samples collected weekly from the Min Jiang, in order to explore the

controlling factors of riverine δ^7Li during catchment weathering and the impacts of hydrology on riverine δ^7Li on the Tibetan Plateau.

2 MATERIALS AND METHODS

2.1 Study Area

The Min Jiang ("Jiang" means "river" in Chinese) catchment (**Figure 1**) is situated at about 28°–33° N and 100°–104° E, and is limited by the Qionglai Mountains in the west and the Min Mountains in the east. The main stream catchment area is 45,500 km^2 (Liu et al., 2020). The Min Jiang, as a tributary of the upper Yangtze River, is a 1279-km-long river sourced from the eastern edge of the Tibetan Plateau at an altitude of 4,579 m, with an elevation gradient of 3,560 m (Ren and Luo, 2013). The mainstream of the Min Jiang flows toward the southern direction with a rich network of tributaries, passing through Maoxian in Longmen Mountains and entering the plain of the Sichuan Basin near Dujiangyan. A significant elevation change is observed when it meets the Sichuan Basin, an alluvial plain with an average altitude of ~500 m. After entering the plain, the Min Jiang main channel joins the Qingyi Jiang at Leshan, and finally imports to the Yangtze River at Yibin.

There are two main tributaries in the upper reaches of the Min Jiang: the Heishui and the Zagunao Rivers (**Figure 1**). Both the tributaries flow toward east and import into the Min Jiang main channel. The Heishui River is 122 km in length with an elevation gradient of 1,048 m, and its catchment area (7,240 km^2) occupies about 31% of the Min Jiang upstream catchment, with an average water discharge (Q_w) of 140 m^3/s. The Zagunao River is 158 km lengthy and has 3,092 m elevation gradient, with a catchment area of 4,629 km^2 and 9.9–122 m^3/s of Q_w. The river water sampling site, the Weizhou hydrological station, is located at 31°28′48.63″N, 103°34′57.86″E in the upper reaches of the Min Jiang, below the confluences of the Zagunao River and the main channel. The catchment area upstream from the station is 18,921 km^2 (Bureau of Hydrology, 2010).

The Min Jiang catchment is located at the junction site among the Songpan-Ganzi fold belt, the west Qin Mountain orogenic belt, and the Longmen Mountain structural belt. The catchment appears to be a parallelogram inset in the Longmen Shan and the Min Mountain tectonic zone (Zhang et al., 2006). The geology of the region is dominated by bedrocks with aluminosilicate minerals, including metamorphic argillaceous sandstone and flysch, granite and monzonitic granite, and detrital sediments, as well as limestones (Jin et al., 2016). At the west side of the Min Jiang, the Songpan-Ganzi fold belt extensively develops Mesozoic flysch sedimentary formations (5–15 km thickness), within which metamorphic sandstone and limestone are dominant lithologies, with a minority of regional developed Indosinian intrusive granites, as well as minor outcrops of sandstone and mudstone interbedded with coal seams (Yoon et al., 2008). At the Longmen Mountain structural belt, the hypo-metamorphic Paleozoic basement is dominant, including slate and phyllite with intercalated marble, carbonate with clastic rocks, or coal-bearing silicates (SLCCC, 1998). From the source of the Min Jiang to north Maoxian, the riverbed is mainly Mesozoic flysch with little lithologic variation, while from Maoxian to the Dujiangyan stretch, the river bedrock is extensively made of Paleozoic complex formed in the Longmen Mountain structural belt (Zhang et al., 2006).

The climate of the Min Jiang catchment is mainly subtropical, and its upper reaches belong to a high elevation plateau climate characterized by low average temperature and little precipitation (Qin et al., 2006; Yoon et al., 2008). The rainfall of the most Min Jiang catchment is carried by Asian and Indian summer monsoons, with 75% of annual precipitation (600–1,100 mm/year) from May to October. In 2010, the annual precipitation in the whole Min Jiang catchment ranged from 455.6 to 2,782.7 mm. The annual Q_w of the Min Jiang was 1.06×10^{10} m^3 in 2000–2011 (Jin et al., 2016). In addition, the average winter and summer temperatures are 0.5°C and 15–17°C for the upper reach region but 5.5 and 26°C for the lower reach plain area in historical records before 2008, respectively (Yoon et al., 2008).

2.2 Samples and Analyses

A total of 71 river water samples were collected weekly from 7 December 2009 to 27 December 2010 at the Weizhou hydrological station. Among them, samples were collected densely during heavy rainfalls: The samples of WZ10-25 to 27 were collected on 27 May 2010, WZ10-29 to 30 were sampled on 7 June, WZ10-36 to 40 were sampled on 17 July, and WZ10-46 to 47 were sampled on 21 August. These samples were used to catch the signature of hydrological changes in river water chemistry and δ^7Li. Also, two rainwater samples were collected in the post-monsoon season in 2010. Three groundwater samples were collected from upstream of the station in November 2020, including one well water sample (W1: 31°26′35.86″N, 103°32′28.43″E), and two spring water samples S2 (31°23′56.27″N, 103°03′8.38″E) and S3 (31°30′20.98″N, 103°12′39.58″E) that just gashed out the surface.

The middle reaches of the Min Jiang experienced moderate numbers of earthquake-triggered landslides induced by the M_w 7.9 Wenchuan earthquake on 12 May 2008. The earthquake triggered tens of thousands of landslides (Li et al., 2014) which increased suspended sediment and solute flux in the Min Jiang in the years that followed (Wang J. et al., 2015; Jin et al., 2016). In order to assess the potential impact of earthquake-triggered landslides on water chemistry, two samples of landslide seepage were collected near Yingxiu in 2018: X1 was the surface runoff on a landslide slope, and X2 was the bottom stream seeped through the landslide mass.

For each river, rain, and groundwater sample, temperature, pH, and TDS (total dissolved solids) were measured at the sampling spot synchronously during the collection. All samples were filtered *in situ* though 0.2 μm Whatman® nylon filters and then collected into two types of polyethylene bottles: one 60 ml fraction was for cation analysis, in which bottles were pre-cleaned with 6 mol/L double-distilled HNO_3 and acidified to pH < 2 by proportionally adding the same pre-cleaned HNO_3 into the samples. The other 30 ml fraction contained a filtered but unacidified sample for anion analysis. All bottles were filled

without air, wrapped with a sealing film, and stored in a 3°C depository to keep from deterioration before treatment.

For the river and rain water samples, major cations (K^+, Na^+, Ca^{2+}, and Mg^{2+}) were analyzed by the Leeman Labs Profile inductively coupled plasma atomic emission spectrometer (ICP-AES), with the relative standard deviation (RSD) less than 1%. Major anions (F^-, Cl^-, and SO_4^{2-}) were measured by ion chromatography (ICS 1200) with 2% RSD, and NO_3^- was measured by a Skalar continuous flow analyzer with 2.2% RSD. The experiments aforementioned were completed at the Nanjing Institute of Geography & Limnology, Chinese Academy of Sciences (CAS). Alkalinity (expressed as HCO_3^-) was measured by a Shimadzu Corporation total organic carbon analyzer (TOC-V_{CPH}) at the Northwest Argriculture and Forestry University, with the RSD less than 1.5%. Li concentrations of these water samples were conducted at the State Key Laboratory of Loess and Quaternary Geology (SKLLQG) in the Institute of Earth and Environment, CAS (IEECAS) using a PerkinElmer NexION 300D Inductively Coupled Plasma Mass Spectrometry (ICP-MS) with the RSD better than 5%.

Pretreatment for the purification of Li was carried out in an ultraclean lab (100 classes in operating window) following the method developed by Gou et al. (2018). Briefly, it was a one-step purification procedure for Li and then an accurate and high-precision determination of its isotopic compositions by MC-ICP-MS (multi-collector inductively coupled plasma mass spectrometer) at IEECAS. First, water samples containing 100–200 ng Li were dried and transformed into 0.5 mol/L HNO_3 solution. Then all the solute samples were purified by a single-step cation exchange chromatographic column filled up with 8 ml resin (Bio-rad AG50W X-12, 100–200 mesh), with 0.5 mol/L diluted HNO_3 as an eluent. The purified Li fraction was extracted in 2% HNO_3 for MC-ICP-MS measurement. Splits collected before and after the main Li elution peak were analyzed for Na and Li contents, to ensure full column recovery. Li recoveries were measured by PerkinElmer NexION 300D ICP-MS and yielded >99.9% recoveries for all samples. The weight Na/Li ratios in all samples were less than 1, which ensured qualified standard deviations and negligible matrix effect during Li isotopic ratio measurements (Gou et al., 2017; Gou et al., 2018; Gou et al., 2020). Li isotope compositions were measured by ThermoFisher NeptunePlus MC-ICP-MS with the standard deviation (s.d.) less than 0.25 and the total procedural blank below 0.3 ng Li. The standard-sample bracketing (SSB) method was used in the measurement with NIST LSVEC as isotopic standard. The results were normalized to LSVEC as follows:

$$\delta^7\mathrm{Li}\ (‰) = 1000 \times \left[\frac{\left(\frac{^7\mathrm{Li}}{^6\mathrm{Li}}\right)_{\mathrm{sample}}}{\left(\frac{^7\mathrm{Li}}{^6\mathrm{Li}}\right)_{\mathrm{LSVEC}}} - 1\right]. \quad (1)$$

Each sample was measured in triplicate to determine average values with RSD. Standards were run together with the samples to verify precision and reliability of the measurements, including the standard of the Isotopic Geochemical laboratory of University of Science and Technology of China (USTC-L, with δ^7Li = −19.3 ± 0.2‰), standard of SPEX CertiPrep (SPEX-Li, with δ^7Li = +12.2 ± 0.2‰), seawater standard (NASS-6, with δ^7Li = +31.1 ± 0.7‰), and Li element standard GBW(E)080547 (δ^7Li = +8.3 ± 0.2‰). The long-term external reproducibility of Li isotope testing was better than ±0.9‰ (2 s.d.), with less than 100 ng sample consumption (Gou et al., 2018), and Li isotope standards tested were in agreement with the values stated previously and from previous studies (e.g., Rudnick et al., 2004; Chetelat et al., 2008; Wang et al., 2015; Pogge von Strandmann et al., 2016), with the trueness better than 2% within 0.5‰ isotopic value errors. Similar analysis methods were operated for landslide seepage samples at Nanjing University and groundwater samples at SKLLQG, IEECAS, respectively.

3 RESULTS

3.1 Hydrology and Water Chemistry

The hydrological and chemical data of the Min Jiang water during December 2009 and December 2010 are listed in **Table 1**. The air temperature (T) increased with fluctuations from middle January to middle August, and then decreased in a similar pattern until the end of 2010 (**Figure 2**), with a minimum of 1.1°C in December and a maximum 29.5°C in August. From May to October (the monsoon season), most of the daily air T were above 15°C. The whole year river water T ranged from 4.0 to 19.5°C, with the lowest value in January and the highest in August (**Figure 2**), a similar trend as the air T but with less fluctuation. The TDS ranged from 169.6 to 435.6 mg/L, with the lowest TDS in July and the highest in November, all within the range of the source region of the Yangtze River (50–3,012 mg/L) (Liu M. et al., 2021). The 2010 annual Q_w was 328.0 m^3/s in average and had a distinct difference between monsoon and non-monsoon seasons: the Q_w ranged from 53.4 to 390.0 m^3/s in the non-monsoon season and 228.0 to 1,500.0 m^3/s in the monsoon season. The minimum Q_w in the monsoon season was about two times higher than the average of the non-monsoon seasons. The Q_w kept a stable and relatively low value from January to April, and increased abruptly under strong rain when stepping into the monsoon season in May. In the monsoon season, the Q_w responded directly to the rainfall intensity, and high Q_w reflected the frequent rainfall in the Min Jiang catchment. A stormy event in 8 June generated the maximum Q_w (1,500.0 m^3/s). After the monsoon season, the Q_w quickly returned to lower values and remained stable for the rest of the year (post-monsoon season).

The water chemistry of river dissolved loads in the Min Jiang was closely related to the monsoon climate (**Figure 3**). First, all ions had a similar variation trend through different seasons: they remained stable at relatively high values in the pre-monsoon season, dropped to a lower and stable level in the monsoon season, and run ups and downs in the post-monsoon season. Second, Q_w variations impacted ion concentrations. The ions showed both dilution and chemostatic behaviors (Koger et al., 2018). As Q_w increased from 50 to 400 m^3/s in the non-monsoon seasons, ionic concentrations decreased rapidly, showing an inverse relationship with Q_w (**Figure 4**). During the monsoon season, there was a less rain interval in middle July to middle

TABLE 1 | Ionic and lithium isotopic compositions of all water samples collected within the Min Jiang river catchment.

Sample type	Sample	Date	TDS	Temp	pH	[Li]	δ^7Li	K^+	Na^+	Ca^{2+}	Mg^{2+}	Cl^-	F^-	NO_3^-	HCO_3^-	SO_4^{2-}
		Y/M/D	mg/L	°C		μmol/L	‰	μmol/L	μmol/L	μmol/L	μmol/L	μmol/L	μmol/L	μmol/L	μmol/L	μmol/L
Pre-monsoon river water	WZ09-1	09/12/7	297.4	-	-	1.274	13.53	38.08	258.92	1,083.59	638.13	67.29	4.25	18.55	3,302.67	254.35
	WZ09-2	09/12/14	290.5	-	-	1.324	13.50	38.79	305.34	1,115.97	675.98	70.16	4.27	19.34	3,165.00	234.43
	WZ09-3	09/12/21	281.5	4.1	8.4	1.403	13.71	38.84	310.61	1,084.94	652.23	105.79	4.98	19.37	2,946.00	284.30
	WZ09-4	09/12/28	291.9	4.1	8.4	1.434	13.72	40.48	304.09	1,105.08	678.67	99.65	3.86	17.82	3,120.00	270.41
	WZ10-1	10/1/4	283.8	4.3	8.4	1.437	12.66	35.96	307.37	1,077.33	651.45	97.04	3.87	19.45	3,002.00	280.08
	WZ10-2	10/1/12	299.6	4.1	8.4	1.513	12.76	42.71	348.93	1,130.60	702.49	117.59	4.87	29.27	3,116.00	316.93
	WZ10-3	10/1/18	304.4	4.0	8.4	1.513	13.26	42.10	345.25	1,162.07	725.41	117.00	4.38	33.74	3,024.00	406.92
	WZ10-4	10/1/25	290.6	5.1	8.7	1.467	13.55	39.70	305.77	1,100.12	680.36	85.46	5.39	21.61	3,047.00	309.44
	WZ10-5	10/2/1	292.1	5.8	8.6	1.566	13.28	36.55	289.18	1,096.35	710.64	59.93	4.35	15.13	3,091.00	308.47
	WZ10-6	10/2/8	291.5	9.7	8.3	1.554	13.16	38.10	318.14	1,104.33	693.38	112.54	4.09	15.44	3,043.00	306.56
	WZ10-7	10/2/15	294.7	11.7	8.3	1.535	13.63	37.30	298.96	1,103.92	702.46	86.97	5.34	20.09	3,129.00	290.01
	WZ10-8	10/2/22	289.9	8.0	8.3	1.591	13.57	38.43	305.68	1,092.35	706.95	71.62	4.00	20.02	3,045.00	308.39
	WZ10-9	10/3/1	299.3	11.7	8.3	1.596	13.81	39.58	330.23	1,123.62	726.01	72.69	4.52	19.96	3,163.00	305.76
	WZ10-10	10/3/9	311.9	6.3	8.4	1.651	13.74	41.18	373.55	1,123.30	732.58	127.24	4.31	7.78	3,209.00	374.92
	WZ10-11	10/3/15	302.5	10.0	8.7	1.680	13.48	43.33	328.16	1,131.99	754.27	86.92	4.27	21.76	3,171.00	316.70
	WZ10-12	10/3/22	298.0	10.9	8.6	1.608	13.63	40.92	324.91	1,113.83	709.71	88.42	3.67	15.44	3,088.00	342.52
	WZ10-13	10/3/28	300.4	9.2	8.7	1.585	14.20	41.63	351.51	1,088.25	718.20	104.69	4.07	18.86	3,141.00	328.39
	WZ10-14	10/4/6	286.8	10.7	8.4	1.502	13.63	41.32	391.77	1,050.50	651.90	153.22	4.92	12.39	2,956.00	310.31
	WZ10-15	10/4/12	271.8	10.7	8.3	1.418	13.55	39.88	303.58	1,030.01	616.43	83.12	4.46	22.00	2,871.00	273.10
	WZ10-16	10/4/19	298.7	11.7	8.7	1.522	14.29	48.11	340.66	1,126.08	689.38	112.45	4.87	15.87	3,005.00	387.03
	WZ10-17	10/4/26	219.7	10.8	8.5	1.339	14.02	44.24	320.88	1,011.59	566.46	111.06	5.33	-	2,029.00	269.16
	WZ10-18	10/5/3	261.1	13.9	8.6	1.278	13.91	36.24	276.77	1,008.24	592.14	72.72	3.24	21.01	2,832.00	214.87
Monsoon season river water	WZ10-19	10/5/9	202.0	11.3	8.8	0.902	12.58	24.34	193.10	884.66	429.29	62.26	-	-	2,100.00	187.35
	WZ10-20	10/5/10	211.2	11.3	8.1	0.979	13.59	23.46	190.72	889.45	455.76	50.25	7.78	-	2,210.00	211.46
	WZ10-21	10/5/17	189.6	11.3	8.5	0.784	14.01	18.51	159.65	796.82	379.50	41.76	7.78	1.34	2,029.17	172.37
	WZ10-22	10/5/21	187.1	12.4	8.6	0.762	13.86	22.69	142.21	827.45	344.51	41.90	8.66	1.64	1,815.00	281.67
	WZ10-23	10/5/22	186.4	12.4	8.6	0.742	14.09	21.49	140.84	820.79	342.10	36.27	8.64	-	1,816.67	279.75
	WZ10-24	10/5/24	195.7	12.4	8.6	0.760	14.23	20.16	164.91	837.75	405.52	45.28	6.94	-	2,057.50	191.01
	WZ10-25	10/5/27	178.4	13.8	8.8	0.788	13.13	25.85	153.31	785.69	308.05	45.47	7.48	-	1,746.67	253.72
	WZ10-26	10/5/27	178.6	13.9	8.8	0.804	12.89	31.68	152.78	795.31	311.93	57.65	7.94	-	1,734.17	253.21
	WZ10-27	10/5/27	196.4	14.1	8.7	1.060	10.48	34.28	201.22	897.28	329.98	69.98	8.46	-	1,845.00	303.50
	WZ10-28	10/6/1	207.0	12.1	8.5	0.830	13.67	20.97	162.94	855.96	419.25	44.90	7.43	25.44	2,228.33	189.29
	WZ10-29	10/6/7	187.5	12.4	8.7	0.714	13.74	29.01	138.18	780.94	366.22	48.06	6.31	16.00	2,034.17	156.22
	WZ10-30	10/6/7	219.7	13.4	8.6	1.098	10.66	39.92	173.36	983.33	390.26	57.72	9.22	3.18	2,300.00	211.34
	WZ10-31	10/6/14	199.2	12.6	8.6	0.867	11.11	23.24	145.01	928.62	331.06	44.64	8.48	12.31	2,140.00	159.51
	WZ10-32	10/6/21	181.2	14.3	8.7	0.783	12.31	24.74	134.97	798.75	340.95	43.69	7.76	13.47	1,937.50	154.43
	WZ10-33	10/6/28	193.0	14.5	8.7	0.859	13.98	28.29	162.02	835.69	392.57	63.67	7.46	3.91	2,046.67	163.44
	WZ10-34	10/7/5	174.1	15.4	8.6	0.714	16.30	20.39	143.51	757.44	327.37	36.21	8.98	-	1,864.17	150.46
	WZ10-35	10/7/12	188.2	13.6	8.2	0.775	13.33	19.15	144.80	799.71	371.32	31.72	7.93	-	2,052.50	150.17
	WZ10-36	10/7/17	190.0	14.1	8.4	0.868	11.74	22.72	158.99	815.21	363.76	42.31	7.97	7.15	2,039.17	162.91
	WZ10-37	10/7/17	169.8	14.2	8.2	0.753	12.25	21.65	126.01	735.87	311.76	32.68	7.47	7.03	1,822.50	148.93
	WZ10-38	10/7/17	171.9	14.2	8.2	0.779	12.78	22.90	132.35	759.18	316.19	31.10	8.24	13.79	1,829.17	154.30
	WZ10-39	10/7/17	171.5	13.9	-	0.770	12.76	25.26	129.81	748.92	310.55	39.11	6.23	58.15	1,820.00	158.68
	WZ10-40	10/7/17	175.4	13.4	8.1	0.789	13.01	22.66	128.56	816.92	333.73	30.89	8.06	-	1,862.50	140.57
	WZ10-41	10/7/19	169.6	14.3	8.1	0.764	13.70	22.62	139.27	763.39	316.66	29.21	7.52	11.34	1,804.17	143.26
	WZ10-42	10/7/26	234.9	13.7	8.1	1.125	13.54	57.10	253.26	951.05	470.49	78.89	8.19	20.43	2,450.83	232.51
	WZ10-43	10/8/2	237.0	15.8	8.1	1.077	13.38	56.75	252.00	951.19	470.12	77.86	6.50	21.84	2,483.33	233.55

(Continued on following page)

TABLE 1 | (*Continued*) Ionic and lithium isotopic compositions of all water samples collected within the Min Jiang river catchment.

Sample type	Sample	Date	TDS	Temp	pH	[Li]	δ^7Li	K^+	Na^+	Ca^{2+}	Mg^{2+}	Cl^-	F^-	NO_3^-	HCO_3^-	SO_4^{2-}
		Y/M/D	mg/L	°C		μmol/L	‰	μmol/L	μmol/L	μmol/L	μmol/L	μmol/L	μmol/L	μmol/L	μmol/L	μmol/L
	WZ10-44	10/8/9	233.5	19.5	8.2	1.115	14.16	24.15	199.30	971.24	515.55	44.41	7.72	18.92	2,404.17	267.46
	WZ10-45	10/8/16	194.7	14.7	8.2	0.891	13.18	22.29	167.50	807.10	407.40	34.22	8.85	12.97	2,061.67	190.33
	WZ10-46	10/8/21	185.1	13.5	8.5	0.813	14.50	24.03	146.22	781.26	371.29	32.19	6.85	18.68	1,935.83	195.74
	WZ10-47	10/8/21	187.7	13.1	8.4	0.791	15.24	30.58	148.16	782.94	369.25	41.92	6.72	2.00	1,965.83	196.69
	WZ10-48	10/8/23	182.6	15.6	8.1	1.274	10.60	22.44	149.54	620.29	363.32	32.47	8.31	-	2,070.00	164.67
	WZ10-49	10/8/30	228.9	16.1	8.5	1.456	12.15	26.99	212.54	952.40	468.15	59.13	8.18	27.16	2,301.67	293.05
	WZ10-50	10/9/6	210.4	14.4	8.5	1.154	12.21	22.58	170.47	900.00	423.49	42.11	7.24	15.48	2,207.50	214.76
	WZ10-51	10/9/13	219.2	16.4	8.5	1.126	12.71	23.71	190.85	929.14	453.66	51.61	7.53	19.91	2,303.33	216.57
	WZ10-52	10/9/20	243.1	12.4	8.1	1.134	14.05	25.68	220.40	983.25	499.87	64.42	8.24	16.43	2,535.83	269.78
	WZ10-53	10/9/27	220.6	13.5	8.5	1.105	13.97	38.33	199.26	920.40	471.40	74.81	7.48	16.27	2,270.00	233.53
	WZ10-54	10/10/4	224.7	13.4	8.6	1.006	15.47	23.63	202.99	920.41	471.47	63.86	6.69	23.18	2,355.83	232.33
Post-monsoon river water	WZ10-55	10/10/11	220.7	12.2	8.6	0.983	14.00	23.18	202.01	916.55	470.94	63.18	7.68	24.56	2,293.33	232.95
	WZ10-56	10/10/18	363.5	11.7	8.1	1.703	15.25	55.36	434.28	1,356.34	760.61	173.23	8.18	75.95	3,012.50	892.84
	WZ10-57	10/10/25	321.9	11.9	8.4	1.454	15.15	80.58	353.41	1,259.56	687.52	179.82	8.34	56.02	2,820.83	648.61
	WZ10-58	10/11/1	381.3	11.9	8.5	1.951	15.16	81.76	565.77	1,553.87	874.88	268.20	-	94.05	3,031.67	875.67
	WZ10-59	10/11/8	409.8	14.3	8.4	2.038	15.77	83.06	607.01	1,639.20	924.25	290.49	25.42	125.47	3,072.50	1,079.68
	WZ10-60	10/11/15	340.9	10.3	8.1	2.078	16.29	83.30	659.96	1,170.59	978.97	316.49	25.84	120.15	1,997.50	1,203.05
	WZ10-61	10/11/22	435.6	13.1	8.1	2.225	16.37	91.02	670.09	1,723.75	997.29	321.83	26.21	136.95	3,143.33	1,218.01
	WZ10-63	10/11/29	308.6	11.4	8.3	2.187	16.12	93.75	642.68	1,672.85	984.93	302.99	-	24.77	1,138.33	1,206.26
	WZ10-64	10/12/6	212.0	11.5	8.3	1.622	16.16	57.99	458.40	1,316.76	761.60	185.04	-	12.39	972.50	616.86
	WZ10-65	10/12/13	318.8	10.9	8.3	2.093	15.77	89.29	646.83	1,698.95	986.18	319.96	-	126.80	1,264.17	1,220.20
	WZ10-66	10/12/20	249.6	11.2	8.7	1.461	15.14	39.45	370.18	1,131.37	669.78	141.15	-	24.55	2,275.00	329.21
	WZ10-67	10/12/27	274.7	9.8	8.6	1.891	15.25	75.90	553.95	1,492.97	887.49	251.37	-	64.21	1,260.83	926.74
Rain water	WZ10-R1	10/03/07	-	-	-	0.248	-	26.24	43.28	176.80	35.26	24.10	13.82	27.46	444.70	101.38
	WZ10-R2	10/04/06	-	-	-	0.249	-	20.68	72.94	230.85	23.21	27.13	12.87	35.15	322.00	160.09
Groundwater	WZ-W1	20/11/25	178.0	11.5	7.6	0.232	16.82	56.05	298.83	1,038.00	661.25	186.13	11.58	53.62	2,213.33	495.98
	WZ-S2	20/11/25	103.0	10.1	7.9	0.313	20.70	60.15	121.83	813.25	143.13	15.24	7.68	25.91	1,475.83	139.43
	WZ-S3	20/11/25	72.0	6.8	7.8	0.370	19.54	33.15	94.26	487.75	102.17	6.42	2.56	13.71	985.83	65.90
Landslide seepage	WZ-X1	18/11/17	-	-	-	0.140	17.10	12.06	138.74	666.25	69.88	45.79	13.98	274.74	640.00	223.49
	WZ-X2	18/11/17	79.0	11.7	8.3	0.145	14.70	12.31	140.17	658.50	70.13	44.63	9.82	258.40	640.00	230.23

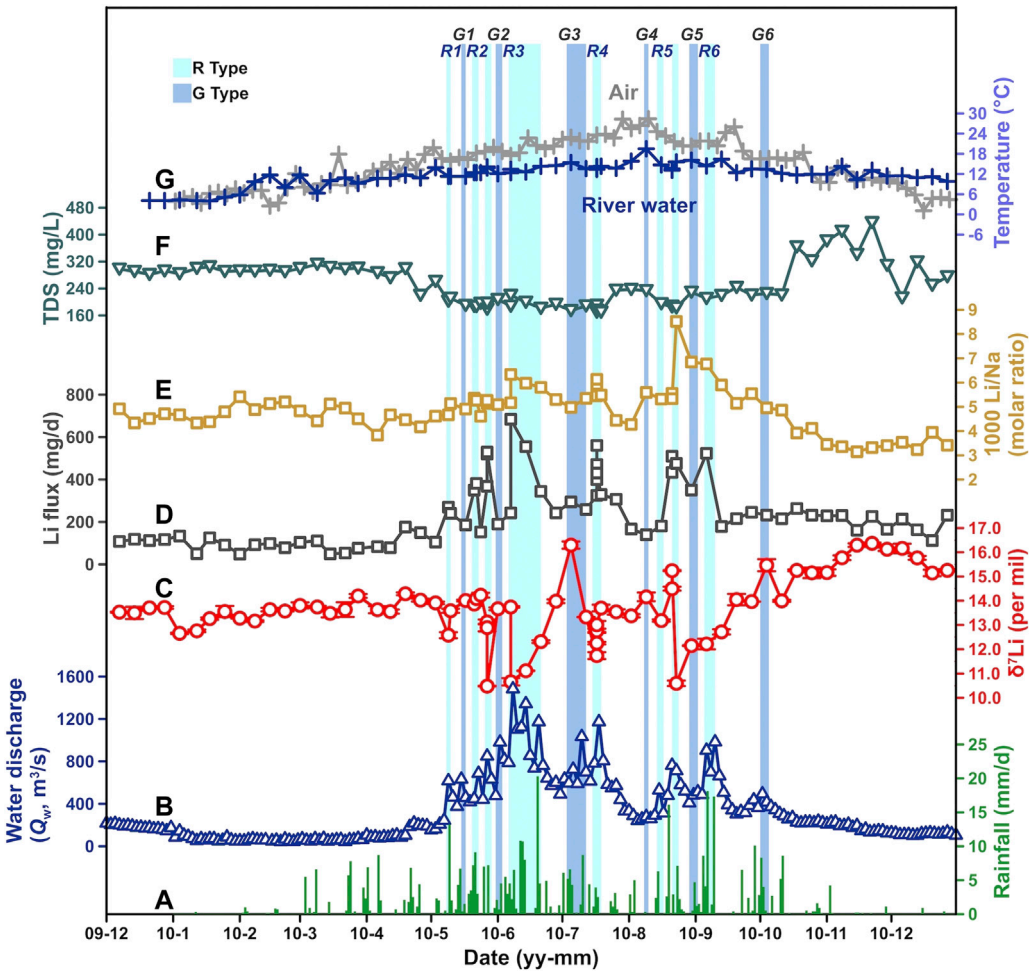

FIGURE 2 | Seasonal variations in **(A)** rainfall, **(B)** river water discharge (Q_w), **(C)** δ^7Li, **(D)** Li flux, **(E)** Li/Na, **(F)** TDS (total dissolved solid), and **(G)** water and air temperature **(T)** at the Weizhou hydrological station over 2010, all showing obvious seasonality. Light and dark blue narrow shades labeled "R" and "G" with numbers represent the R- and the G-type waters, among which R2 and R5 contain two short intervals.

August in which the ionic concentrations increased slightly (**Figure 3**). When Q_w rose continually to >400 m^3/s during the monsoon season, there was less dilution effect on ionic concentrations (**Figure 4**), suggesting an excess input under intense water flow. The ionic concentrations in the post-monsoon season were not as stable as those in other seasons. They increased with fluctuation, and dropped back with undulations to low values near the pre-monsoon season at the end of the year.

3.2 Li Concentrations and Li Isotopes

Li concentrations ([Li]) and δ^7Li values of all Min Jiang water samples are listed in **Table 1**. Over 2010, the dissolved [Li] in the Min Jiang ranged from about 0.714 μmol/L (during the monsoon season) to 2.225 μmol/L (during the non-monsoon seasons) with an average of 1.266 μmol/L, which is much higher than the world's average riverine [Li] (0.22 μmol/L) (Hu and Zhou, 2012; Liu et al., 2021). These values were generally higher than those of many rivers around the globe, such as the Amazon River with [Li] from 0.06 to 1.67 μmol/L (Dellinger et al., 2015), the Mackenzie River from 0.02 to 1.29 μmol/L (Millot et al., 2010a), and the Orinoco River from 0.01 to 0.81 μmol/L (Huh et al., 2001), but overall, they were relatively lower than those of the Yangtze River main channel, in which [Li] ranged from 0.42 to 4.57 μmol/L (Wang et al., 2015). The [Li] of groundwater in the Min Jiang catchment ranged from 0.232 to 0.370 μmol/L, within the range of the world groundwater [Li] ranging from 0.01 to 28 μmol/L depending on different settings (Su, 2012; Mayfield et al., 2021). Rainwater [Li] were generally low, reported to be 0.004–0.292 μmol/L (Millot et al., 2010b). The [Li] in the rainwater of the Min Jiang catchment were 0.248 and 0.249 μmol/L. The [Li] of landslide seepage samples were even lower, 0.140 (X1) and 0.145 μmol/L (X2) (**Table 1**).

Over the sampling period, the dissolved δ^7Li in the Min Jiang ranged from +10.48‰ in monsoon season to +16.37‰ in

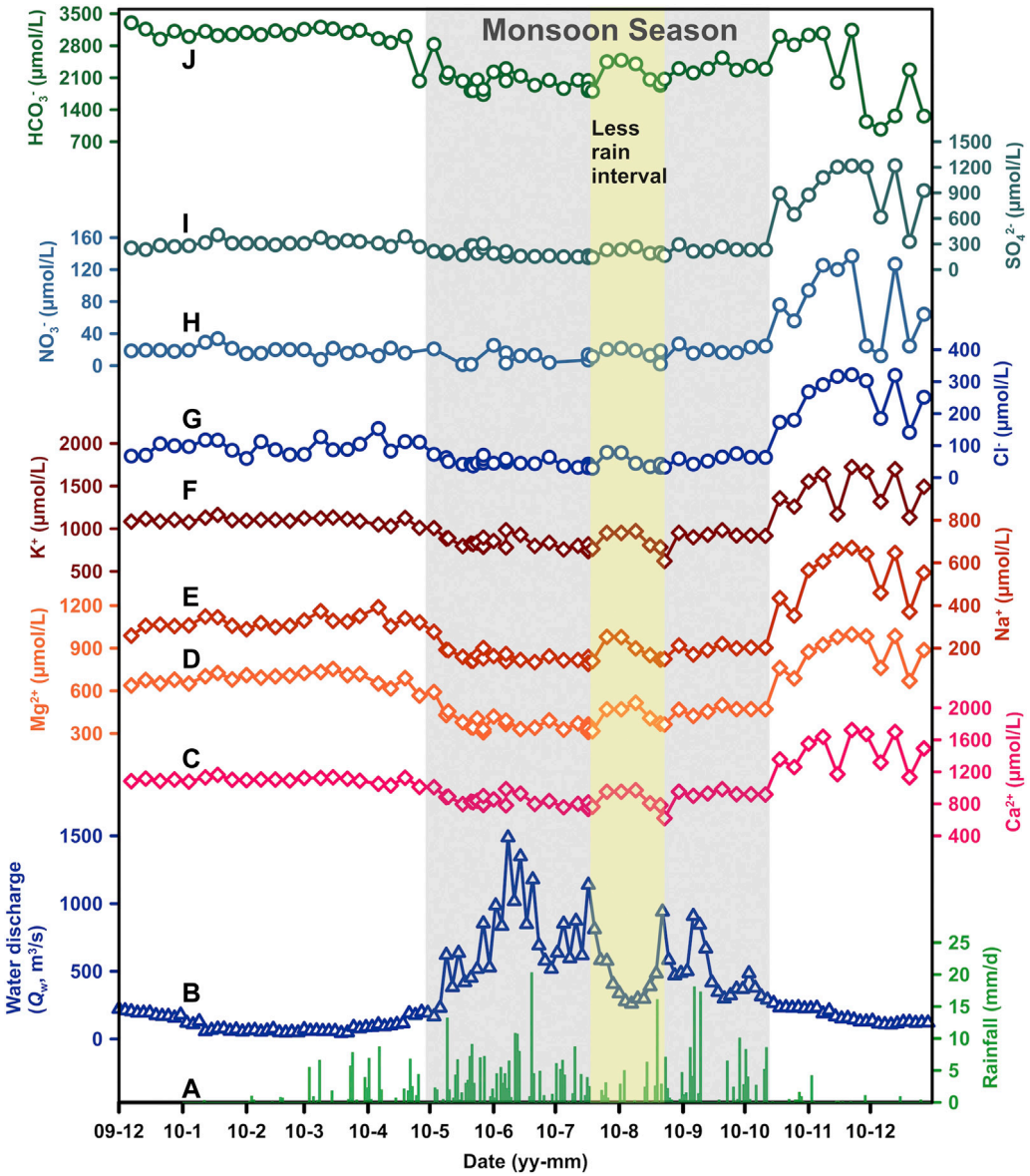

FIGURE 3 | Seasonal variation of major ions for the Min Jiang river waters, including **(C)** Ca^{2+}, **(D)** Mg^{2+}, **(E)** Na^{+}, **(F)** K^{+}, **(G)** Cl^{-}, **(H)** NO_3^{-}, **(I)** SO_4^{2-}, and **(J)** HCO_3^{-}, along with **(A)** rainfall and **(B)** water discharge (Q_w). The monsoon season is shaded by gray, with a relatively less rain interval during mid-July and mid-August shaded by faint yellow.

the non-monsoon seasons, covering a narrower range than the spatial δ^7Li variation in the Yangtze River (ranging from +7.6 to +42.1‰) (Wang et al., 2015) and other global rivers (ranging from +1.2 to +42.1‰, with an average +23.4‰) (Liu et al., 2021). The δ^7Li values of two groundwater samples in the Min Jiang catchment were +16.82 and +20.70‰, respectively, within the range of the reported global groundwater δ^7Li (+6.7 to +28.6‰) (Hu and Zhou, 2012; Su, 2012; Liu et al., 2021; Mayfield et al., 2021). Close to those of the groundwater samples, two landslide seepage samples had δ^7Li values of +17.1 and +14.7‰, respectively.

The riverine Li flux and δ^7Li also showed significant seasonal variations in response to the Q_w in the Min Jiang through time in 2010. As shown in **Figure 2**, Li flux and δ^7Li remained in invariant levels until the beginning of the monsoon season. During the monsoon season, with the increasing Q_w, Li flux increased owing to strong weathering, with large fluctuations. Along the time that the monsoon ended, Li flux returned to the level of the monsoon's beginning. Similarly, δ^7Li fluctuated dramatically with Q_w during the monsoon season, and turned to a stable level, with relatively higher values than the pre-monsoon season. One of the most interesting observations is

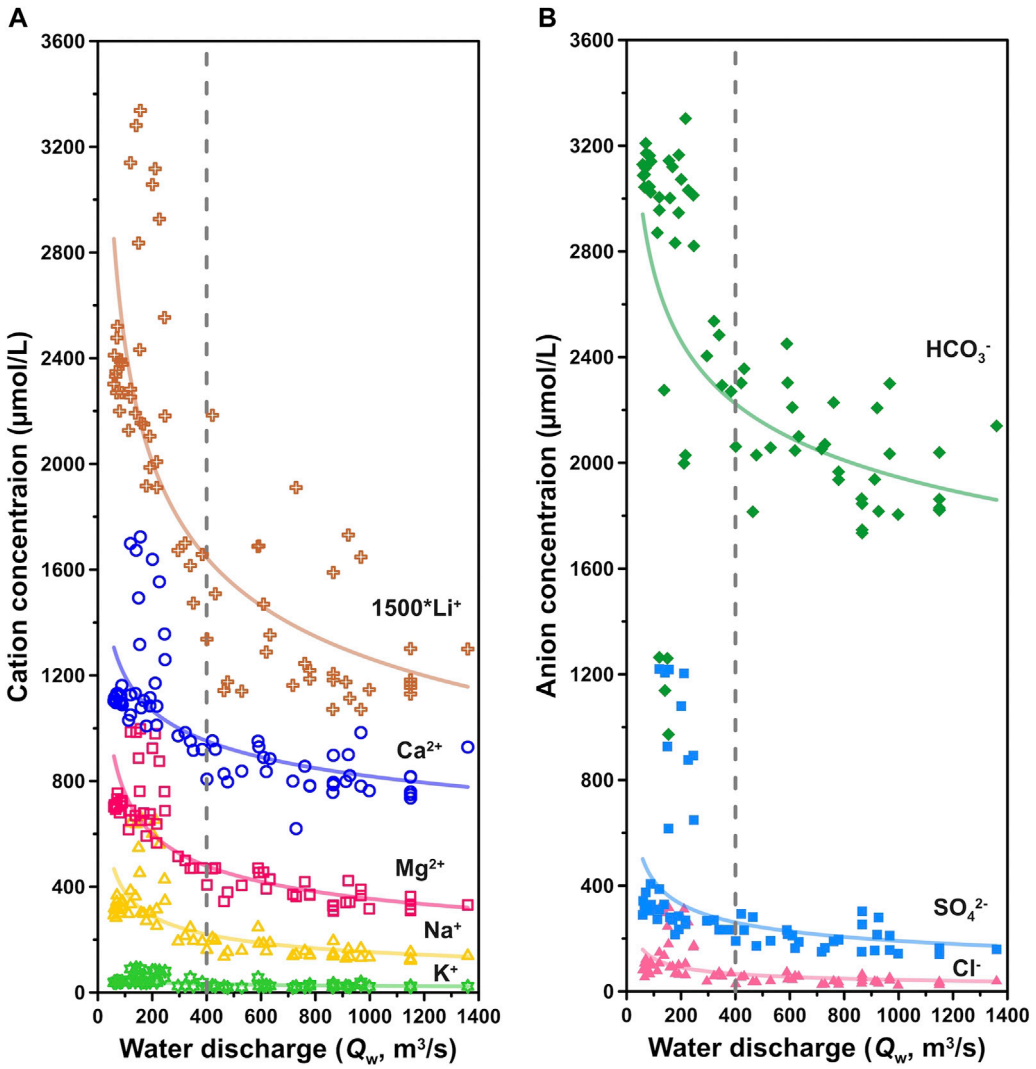

FIGURE 4 | Changes of **(A)** cation and **(B)** anion concentrations with water discharge (Q_w). Q_w at 400 m^3/s as a boundary marked gray dashed lines, where below 400 m^3/s the ionic concentrations are strongly affected by the dilution effect, whereas above 400 m^3/s the riverine ion concentrations are less affected by increasing Q_w.

that both Li flux and δ^7Li in the Min Jiang waters exhibited not only seasonal variation but also sensitive response to hydrological changes as discussed in the following text.

3.3 Riverine δ^7Li Responses to Hydrological Changes During the Monsoon Season

During the monsoon season in 2010, there were several strong rainfall intervals with high Q_w, interrupted by a less rain interval (**Figures 2**, **3**). During the strong rainfall intervals, the Min Jiang waters were characterized by decreased δ^7Li but increased Li flux relative to their neighbours (as shaded by light blue in **Figure 2**). Since these waters were associated with strong rainfall, we defined them as the "R-type" water. There were six intervals with the R-type waters, marked as R1 to R6 in **Figure 2**, in which R2 and R5 consisted of two short intervals. In each R-type water interval, when Q_w went up, riverine δ^7Li decreased abruptly. Meanwhile, its Li flux reached a high value at the moment and then quickly dropped back to a lower value. For instance, in the R4 interval, the Q_w increased from 615 to 1,190 m^3/s and δ^7Li dropped nearly 1.5‰ (from +13.33 to +11.74‰), while Li flux increased from 258.7 to 560.8 mg/day.

Between the R-type water intervals, there were another six intervals characterized by increased δ^7Li but decreased Li flux relative to their neighbours (as shaded by dark blue in **Figure 2**), in contrast to the R-type waters. In each interval, Q_w rose slightly and riverine δ^7Li increased, corresponding to lower Li flux than before and after it. Considering that the high δ^7Li may be affected by the input of groundwater and/or landslide seepage, both with higher δ^7Li, as discussed in the following text, these waters were named as the "G-type" waters, marked as G1 to G6 in **Figure 2**. Take the G4 for an example, it happened during the less rain period of the monsoon season, but its Q_w increased from 228 to 311 m^3/s with little rainfall; the riverine δ^7Li increased from +13.38 to +14.16‰, with Li flux decreasing from 166.8 to 139.6 mg/day.

TABLE 2 | Comparisons of δ^7Li, Li fluxes, and Li/Na ratios between, before, and during the intervals of the R- and G-type waters.

Type water no	Date (2010)		Water discharge Q_w (m^3/s)		δ^7Li (‰)		Li flux (mg/day)		1,000*Li/Na	
	Start date	End date	Before	During	Before	During	Before	During	Before	During
R1	05–09	05–10	301.0	633.0	+13.91	+12.58	105.10	269.50	4.62	5.14
R2-1	05–21	05–23	404.0	926.0	+14.01	+13.86	186.29	381.59	4.91	5.36
R2-2	05–27	05–28	497.0	866.0	+14.23	+10.48	152.65	529.47	4.61	5.27
R3	06–07	06–21	806.0	1,500.0	+13.67	+11.11	189.72	684.26	5.09	6.34
R4	07–16	07–19	615.0	1,190.0	+13.33	+11.74	258.66	560.79	5.35	6.14
R5-1	08–15	08–17	308.0	546.0	+14.16	+13.18	139.59	180.59	5.59	5.32
R5-2	08–22	08–24	698.0	953.0	+15.24	+10.60	433.43	476.04	5.34	8.52
R6	09–06	09–10	538.0	1,000.0	+12.15	+12.21	350.45	523.43	6.85	6.76
G1	05–16	05–17	546.0	650.0	+13.59	+14.01	240.51	186.29	5.14	4.91
G2	06–01	06–03	494.0	998.0	+10.48	+13.67	529.47	189.72	5.27	5.09
G3	07–04	07–12	564.0	1,050.0	+13.98	+16.30	294.62	258.66	5.30	4.98
G4	08–09	08–10	228.0	311.0	+13.38	+14.16	166.76	139.59	4.27	5.59
G5	08–30	09–02	426.0	562.0	+10.60	+12.15	476.04	350.45	8.52	6.85
G6	10–02	10–05	378.0	510.0	+13.97	+15.47	245.87	232.45	5.54	4.96

The value differences of Li flux, riverine δ^7Li, and Li/Na ratios before and during the intervals of the R- and the G-type waters are presented in **Table 2** and **Figure 5**. It demonstrated that riverine Li flux and δ^7Li were clearly impacted by monsoonal hydrological conditions, with two distinct responses as discussed in **Section 4.4** in the following text.

4 DISCUSSION

4.1 Control of Seasonal Variations in Min Jiang Water Chemistry

Similar to river chemistry in the Yangtze River headwaters and the Yellow River (Zhang et al., 2015; Ma et al., 2020), the summer monsoons bring abundant rainfall, resulting in dilution of the riverine ions in the Min Jiang during the monsoon season. A similar seasonal pattern was also observed elsewhere and was related to the Indian monsoon (Galy and France-Lanord, 1999; Tipper et al., 2006). However, when Q_w exceeded 400 m^3/s, the ionic concentrations seemed not to correlate with Q_w (**Figure 4**), suggesting excess input to the river water by intensified weathering and/or groundwater associated with the hydrological events (Zhang et al., 2015), as discussed in the following text. The excess input of Ca^{2+} and HCO_3^- can be further supported by the relation between Ca/Na* versus Mg/Na* ratios (where $Na^* = Na^+ - Cl^-$) at different seasons. As shown in **Figure 6**, lower Ca/Na* and Mg/Na* ratios in the river waters of the non-monsoon seasons were clearly separated from those of the monsoon season, with different slopes. The higher Ca/Na* and Mg/Na* ratios in the river waters of the monsoon season waters than those of the non-monsoon seasons reflected more contribution of carbonate dissolution relative to silicates, supported by higher Ca^{2+} and HCO_3^- in the monsoon season than those in the non-monsoon seasons (**Figure 7**). All these features can be attributed to faster dissolution kinetics of carbonates under monsoon conditions.

4.2 Sources of Major Ions and Li in the Min Jiang

In order to address the δ^7Li signatures of river waters, it is important to determine the sources of major ions and dissolved Li (Vigier et al., 2009). Major reservoirs affecting large river chemistry include dissolution of silicate, carbonate, evaporite, and human inputs (Gaillardet et al., 1999), as well as rainwater (Yoon et al., 2008). We employed the forward model to evaluate the contributions of the major reservoirs, which sequentially allocates the major ions and dissolved Li to their sources (Meybeck, 1987; Gaillardet et al., 1997; Dellinger et al., 2015; Gou et al., 2019).

For atmospheric inputs of major ions, chloride (Cl^-) was used as a reference for the rain correction:

$$X_{\mathbf{rain}} = \left(\frac{\mathbf{X}}{\mathbf{Cl}}\right)_{\mathbf{rain}} \times \mathbf{Cl_{ref}} \quad (2)$$

where X_{rain} represents the concentration of ion X (Na^+, Mg^{2+}, Ca^{2+}, and SO_4^{2-}) derived from rainwater, $(X/Cl)_{rain}$ refers to the measured X/Cl ratio in rainwater, and Cl_{ref} was the lowest Cl^- concentration of the catchment river sample dataset (here 23.0 μmol/L of Cl^- was used from the river water sample at the upper reaches near Zhenjiangguan).

After the correction of atmospheric inputs, we attributed the remaining Cl^- and SO_4^{2-} to evaporite and sulfide (abbreviated as Cl_{eva} and $SO_{4,eva}$) dissolution. Then, the Na^+ and Ca^{2+} proportions from evaporites and sulfides were determined by **Eqs 3**, **4**.

$$\mathbf{Na_{eva}} = \mathbf{Cl_{eva}} = \mathbf{Cl_{dissolved}} - \mathbf{Cl_{ref}} \quad (3)$$

$$\mathbf{Ca_{eva}} = \mathbf{SO_{4,eva}} = \mathbf{SO_{4,dissolved}} - \mathbf{SO_{4,rain}} \quad (4)$$

For silicate dissolution, we considered that all K^+ and the residual Na^+ after the corrections of rain, evaporite, and sulfides were from silicate weathering, abbreviated as K_{sil} and Na_{sil}. Ca^{2+} and Mg^{2+} from silicate dissolution were calculated by multiplying Na_{sil} by Ca/Na (0.54) and Mg/Na (0.26) ratios of local silicate rock compositions (Qin et al., 2006; Yoon et al., 2008).

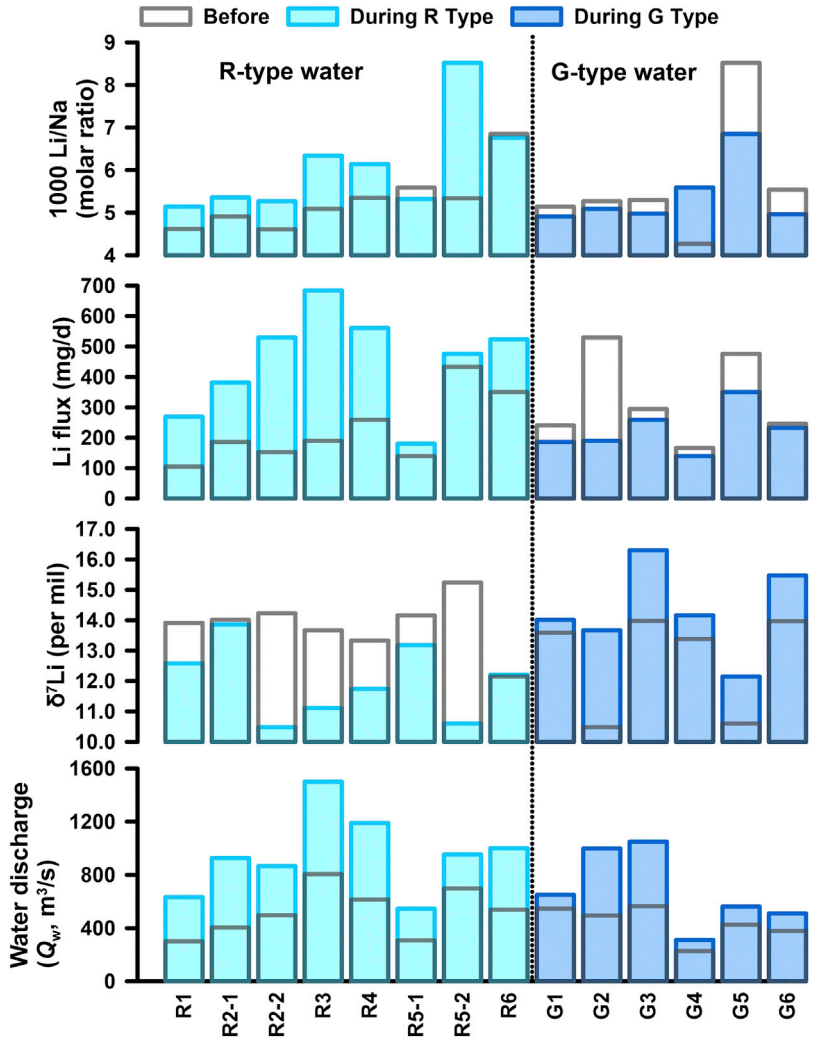

FIGURE 5 | Comparisons of δ^7Li, Li flux, and Li/Na for the R-type and G-type waters with water discharge (Q_w). The values during the intervals with the R-type and G-type waters are plotted by light and dark blue filled rectangles, and the values before the intervals by blank rectangles with gray frames, respectively.

$$\mathbf{Na_{sil} = Na_{dissolved} - Na_{eva} - Na_{rain}} \quad (5)$$

$$\mathbf{K_{sil} = K_{dissolved}} \quad (6)$$

$$\mathbf{Mg(Ca)_{sil} = Na_{sil} \times \left(\frac{Mg(Ca)}{Na}\right)_{sil}} \quad (7)$$

After the aforementioned corrections, the remaining Ca^{2+} and Mg^{2+} were thought to be from carbonate contribution by **Eqs 8** and **9**:

$$\mathbf{Ca_{carb} = Ca_{dissolved} - Ca_{sil} - Ca_{eva} - Ca_{rain}} \quad (8)$$

$$\mathbf{Mg_{carb} = Mg_{dissolved} - Mg_{sil} - Mg_{rain}} \quad (9)$$

The results showed that in the hydrological year of 2010 (four samples of 2009 are not included), the total cations from evaporites and sulfides reached 11.9 ± 6.2% in the pre-monsoon seasons, followed by 9.1 ± 8.8% in the monsoon season, and 27.9 ± 20.7% in the post-monsoon season. This indicated that dissolution of evaporites and sulfides played a more important role in the post-monsoon season than other seasons in the Min Jiang catchment. The contribution of carbonates for cations occupied 56.8 ± 8.1% in the pre-monsoon season, while 59.1 ± 14.1% in the monsoon and 41.8 ± 24.2% in the post-monsoon season. Meanwhile, the silicate contribution for cations was relatively stable through all seasons, with 18.4 ± 3.2% in the pre-monsoon season, 14.0 ± 6.0% in the monsoon season, and 17.7 ± 6.0% in the post-monsoon season.

For Li as a trace element, [Li] in rainwater is low (here 0.25 μmol/L) so that the contribution of atmospheric input to riverine Li^+ is usually assumed to be negligible (Huh et al., 2001; Wang et al., 2015). Here, we used the typical Li/Ca ratio value of ~ $(1.5 \pm 0.5) \times 10^{-5}$ in carbonates (Hathorne and James, 2006; Pogge von Strandmann et al., 2013) and a mean Li/Na value of 3×10^{-5} for evaporites (Kloppmann et al., 2001) to obtain the proportions of Li^+ derived from carbonates and evaporites by

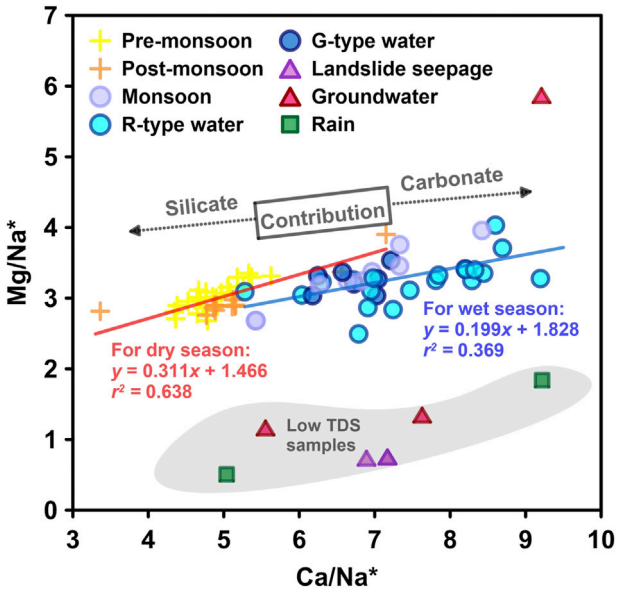

FIGURE 6 | Correlations of Mg/Na* vs. Ca/Na* ($Na^* = Na^+ - Cl^-$) for river water samples from the dry and wet seasons, respectively, also showing rainwater, groundwater, and landslide seepage with low Mg/Na* and TDS.

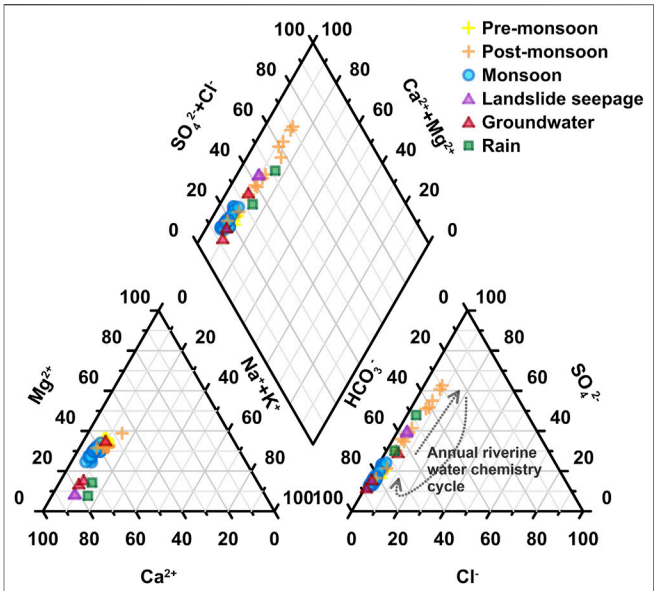

FIGURE 7 | Piper diagrams for ions of river water samples from the Min Jiang catchment. Dark gray dot curves show a surmised annual cycle of anions from pre-monsoon to post-monsoon seasons.

$$\mathbf{Li_{carb}} = \mathbf{Ca_{carb}} \times \left(\frac{\mathbf{Li}}{\mathbf{Ca}}\right)_{\mathbf{carb}} \quad (10)$$

$$\mathbf{Li_{eva}} = \mathbf{Cl_{eva}} \times \left(\frac{\mathbf{Li}}{\mathbf{Na}}\right)_{\mathbf{eva}} \quad (11)$$

The result showed that 0.9 ± 0.8% of dissolved Li^+ was sourced from carbonates and less than 0.4% of Li^+ was from evaporites. The remaining Li^+ after subtracting Li_{eva} and Li_{carb} was considered to be from silicates. The result showed 99.0 ± 0.8% Li^+ from silicates ($[Li]_{sil}$).

4.3 Weathering Rate and Its Relationship With Riverine δ^7Li

Based on the calculations aforementioned, silicate weathering dominated the source of riverine Li^+ in the Min Jiang. The rate of silicate weathering (SWR, mol/km^2/day) was calculated by silicate-derived cations multiplying daily Q_w, and then divided by the total catchment area (A) above the Weizhou hydrological station (18,921 km^2) as the following equation (Zhang et al., 2015):

$$\mathbf{SWR} = \mathbf{Cation_{sil}} \times \frac{\mathbf{Q_w}}{\mathbf{A}} \quad (12)$$

The SWR in the Min Jiang also had distinct seasonal variations. The SWR remained within 161.0 ± 62.5 mol/km^2/day in the pre-monsoon season, and then increased sharply to 523.8 ± 146.2 mol/km^2/day in the monsoon season, with fluctuations by the domination of different types of waters as discussed in the following text. In the post-monsoon season, the SWR declined to 381.2 ± 100.7 mol/km^2/day. Apparently, a higher SWR appeared during the monsoon season, also demonstrated by higher Si/Na* (**Figure 8A**), indicating that monsoon rainfall accelerated silicate weathering (**Figure 8B**). This is consistent with previous findings (Qin et al., 2006; Zhang et al., 2015). This daily SWR was generally within the range of the middle reaches of the Yellow River (~9.5–565.2 mol/km^2/day), which also showed strong weathering in the monsoon season (Zhang et al., 2015). The annual average SWR in upper Min Jiang was 129.1 × 10^3 mol/km^2/year or 3.7 t/km^2/year, within the range of the Yangtze River headwater basins (1.8 to 12 t/km^2/year) (Li S.-L. et al., 2014; Ma et al., 2020), also close to the Mackenzie (0.13–4.3 t/km^2/year) draining the Rocky Mountains in the subarctic (Millot et al., 2003), but less than the Ganga, Yamuna, and Kosi Rivers with higher annual SWR of 8.4, 10.3, and 9.3 t/km^2/year, respectively; however, their tributaries displayed lower values than main channels (Pogge von Strandmann et al., 2017). Moreover, the SWR in the Min Jiang was far less than that of the rivers draining the Andes with a mean value at 22 t/km^2/year (Moquet et al., 2011) but was 4–5 times higher than that of the Austrilian Victorian Alps region (23–31 × 10^3 mol/km^2/year) (Hagedorn and Cartwright, 2009). The CO_2 consumption yield was (186.4 ± 26.4) × 10^3 mol/km^2/year for the Min Jiang catchment area in 2010, which is higher than those of the Yellow River and the Yangtze River.

The δ^7Li of the river dissolved load was considered to be related to the intensity and regime of silicate weathering at the scale of the basin (Vigier et al., 2009; Millot et al., 2010a). Within one hydrological year in the Min Jiang catchment, the SWR was proportional to Q_w (**Figure 8B**), whereas δ^7Li and SWR exhibited a negative correlation, with relatively high δ^7Li and low SWR in the non-monsoon seasons and low δ^7Li and high SWR in the monsoon season (**Figure 8C**). This correlation was consistent with Vigier's empirical law that δ^7Li and SWR fit a negative power

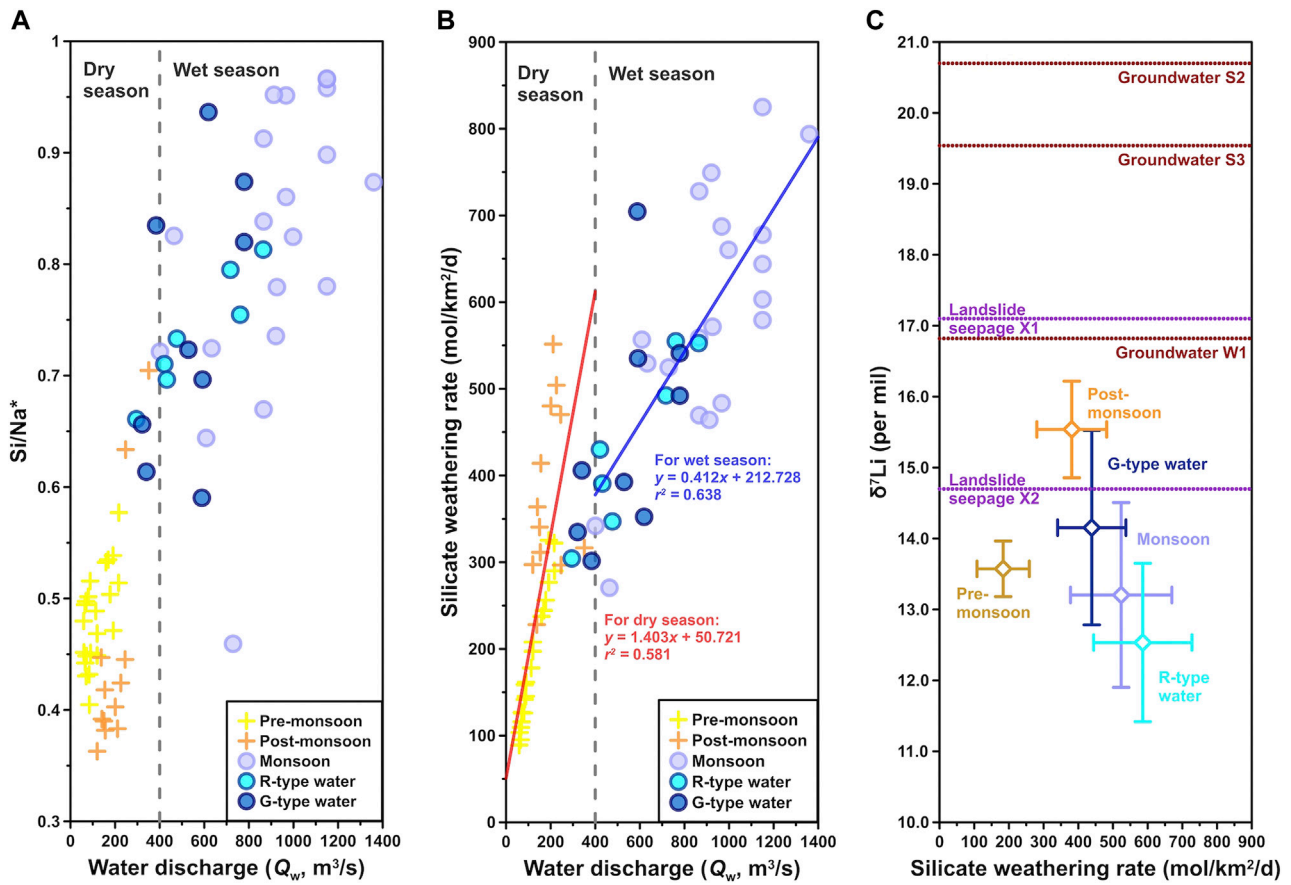

FIGURE 8 | Relations between **(A)** Si/Na* ratio (Na* = $Na^+ - Cl^-$) and **(B)** silicate weathering rate (SWR) vs. water discharge (Q_w), and **(C)** δ^7Li vs. SWR. Following the Q_w boundary in **Figure 4**, gray dashed lines divide into dry and wet seasons. In panel **(C)**, blank diamond symbols with error bars represent average δ^7Li and SWR values for each class of samples. Violet and red dot lines mark δ^7Li values of landslide seepage and groundwater samples, respectively, because they have no SWR data.

function. In fact, similar patterns had been reported by the Amazon, Ganges, Orinoco, Lena, the Yellow River, and the Qiantang River that all displayed (at their outlet) δ^7Li values higher than 21‰ for corresponding chemical erosion rates lower than 14 t/km^2/year (Huh et al., 1998; Gaillardet et al., 1999; Wu et al., 2005; Vigier et al., 2009). It was also reported that tributaries of Himalayan rivers draining silicates had lower dissolved δ^7Li values (by 2.3–4.2‰) following the monsoon when weathering was more intense due to higher runoff and elevated temperatures (Kısakürek et al., 2005).

4.4 Impacts of Hydrology on Riverine Li Isotopes

One of the most interesting observations for the seasonal δ^7Li in the Min Jiang waters is that there are two types of river waters with different responses of the δ^7Li values to hydrology during the monsoon season, as defined previously as the R- and G-type waters (as shades in **Figure 2**). Considering that Li is not involved in terrestrial biological cycles (e.g., Lemarchand et al., 2010; Pogge von Strandmann et al., 2016) and that vegetation within the upper Min Jiang catchment is sparse, $[Li]_{sil}$ should not be affected by biological processes in the Min Jiang. $[Li]_{sil}$ should be dominantly controlled by dilution/evaporation processes at the first order, and then by the balance between silicate weathering and incorporation into secondary minerals.

The R-type waters with low δ^7Li usually appeared during a major rainfall which was caused by the rapid rise of Q_w. The δ^7Li drop was accompanied by an increase in both [Li] and Li flux. The decreased riverine δ^7Li but increased Li flux can attribute to an increase in silicate dissolution during the monsoon season. As the Q_w increased, more dissolved Li^+ was flushed into the river, leading to a rise in the Li flux during the monsoon (**Figures 2**, **5**). It is further supported by increasing Si/Na* and SWR proportional to Q_w (**Figures 8A,B**). However, for the R-type waters, rapidly increased Q_w sped up water flow velocity, meaning relatively short water residence time. The decrease in riverine δ^7Li is most likely due to the increased input of silicate weathering with low δ^7Li and/or a decrease in rates of secondary mineral precipitation during the rain intervals. It means that the δ^7Li in the R-type waters should only equilibrate with the solid. Lowest average δ^7Li but highest SWR values for the R-type waters (**Figure 8C**) further support that riverine δ^7Li is a strong kinetic control (West et al., 2002). After each R-type water

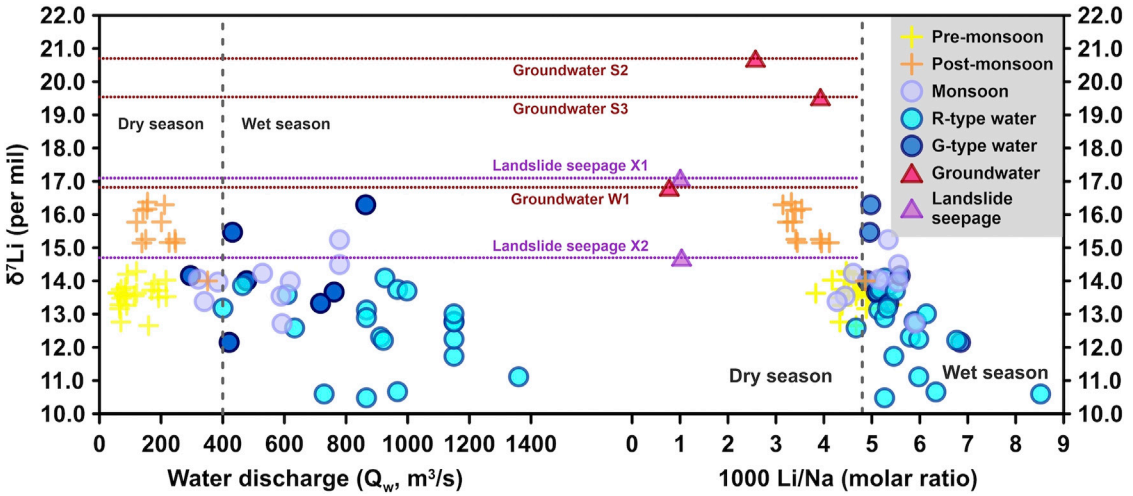

FIGURE 9 | Scatterplots for δ^7Li vs. water discharge (Q_w) and 1,000*Li/Na for river waters in the Min Jiang River. Following Q_w boundary at 400 m^3/s in **Figure 4**, the gray dashed lines divide into dry and wet seasons. As the same as **Figure 7**, violet and red dot lines mark δ^7Li values of landslide seepage and groundwater samples, respectively, because they have no Q_w data.

interval, riverine δ^7Li returned to higher values, which may result from more ^{6}Li incorporation into secondary minerals during the longer water–rock interaction when Q_w decreased (e.g., Lemarchand et al., 2010). This is also supported by laboratory water–rock interaction experiments that showed large (19‰) increases in δ^7Li in solutions over a short period of time (Pogge von Strandmann et al., 2019).

Similar changes of dissolved δ^7Li were observed both in a forested granitic catchment (Strengbach, Vosges Mountains, France) (Lemarchand et al., 2010) and in a highly weathered catchment (Quiock Creek in Guadeloupe archipelago, French West Indies) (Fries et al., 2019). Lemarchand et al. (2010) found that δ^7Li in both a spring and a stream decreased with an increasing Q_w. This was because Li isotopic fractionations occurred during the secondary phase precipitation along the water pathway through the rocks, resulting in high δ^7Li with increasing residence time of waters. Similarly, Fries et al. (2019) found that the δ^7Li values of the river dissolved load in the Quiock Creek catchment decreased by ~2% after the largest rain event and remained low afterward. The decreased δ^7Li was considered due to either input of Li from isolated pockets of soil solution with lower δ^7Li that were flushed out during the rain events, or due to a decrease in rates of secondary mineral (mostly halloysite and kaolinite) precipitation during the rain events. After a rain event, the secondary mineral phase turned unsaturated, consistent with lower rates of precipitation, in which case, either enhanced dissolution of secondary minerals or suppressed secondary mineral formation could result in lower riverine δ^7Li (Fries et al., 2019).

Between the R-type water intervals, there were six intervals with the G-type waters whose Q_w rise was not related to rainfall—sometimes, it was after rainfall (as shaded by dark blue in **Figure 2**). During the G-type water intervals, though Q_w increased, the Li fluxes became low and δ^7Li jumped to higher values relative to their neighbours. Considering that groundwater had higher δ^7Li values than river waters (**Figures 8B**, **9**), it is certainly possible that groundwater affected riverine δ^7Li in the Min Jiang. Groundwaters are typically concentrated in silicate-derived cations (such as Li^+) as a result of prolonged water–rock interaction (e.g., Tipper et al., 2006). Meanwhile, the majority (55–68%) of global groundwater discharge was from silicates in humid, low-latitude, and tectonically active regions, and groundwater derived solute fluxes occupied at least 5% of the riverine fluxes. Therefore, groundwater discharge might play an outsized role in terrestrially derived solute fluxes of silicate weathering and thus the regulation of atmospheric CO_2 (Luijendijk et al., 2020; Mayfield et al., 2021). In mountain areas, the river deeply cuts the valley and groundwater supplies river water. As a result, some rivers even have higher δ^7Li than groundwaters (e.g., Bagard et al., 2015; Liu et al., 2015; Manaka et al., 2017). Since the catchment above the Weizhou hydrological station is located at the mountain areas, discharge of such groundwater could shift river chemistry toward higher δ^7Li (**Figures 8B**, **9**). Meanwhile, seismic landslides triggered by the 2008 Wenchuan earthquakes are prevalent throughout the study region (e.g., Li et al., 2014), which can act as solute generators by producing reactive fine-grained sediment (Wang et al., 2015) and by focusing flow through this material (e.g., Jin et al., 2016). Leaching of exchangeable cations from finely grounded landslide debris could also contribute to the solute load. The landslide mass embraced large porosity in which it gave Li isotope time and physicochemical environment to fractionate, mainly by secondary minerals absorbing ^{6}Li in the pore water, making landslide seepage waters heavy Li isotope signature, but less aqueous Li remained. Indeed, two samples of landslide seepage were at relatively higher δ^7Li values compared to river waters (**Figures 8C**, **9**). On the other hand, the [Li] of both groundwater and landslide seepage were all less than that of river water within the Min Jiang catchment (**Table 1**). When such waters were delivered to the river channel, river water would increase δ^7Li but

decrease Li flux relative to their neighbours, being as a G-type water (**Figure 9**). Higher δ^7Li but lower Li/Na* ratios for the post-monsoon waters (**Figure 9**) probably indicate an excess Li supply of such waters to the Min Jiang relative to the pre-monsoon season. As the monsoon season gradually faded out, the change of strengthened evapotranspiration and oversaturation of clays probably resulted in more ^{6}Li incorporated into clays and higher δ^7Li in the residual pore water (Xu et al., 2021), which might be finally imported into the river as landslide seepage. In addition, the lengthened rock–fluid interaction times during the less rain intervals could simultaneously cause higher riverine δ^7Li (e.g., Bagard et al., 2015; Pogge von Strandmann et al., 2019) as the G-type waters.

5 CONCLUSION

In the Min Jiang catchment along the eastern Tibetan Plateau, seasonally hydrological variation caused by Asian and Indian summer monsoons influences water chemistry and riverine Li isotope compositions. Silicate weathering produced more than 98.2% of the riverine Li. Relative to distinct variation in riverine δ^7Li during the monsoon season, Li isotopic compositions were relatively stable in the pre- and post-monsoon seasons, with overall lower δ^7Li values averaged 13.6‰ in the pre-monsoon season and higher δ^7Li values averaged 15.5‰ in the post-monsoon season. Based on the distinct response of the riverine δ^7Li to increasing Q_w, two types of river waters were distinguished in the Min Jiang during the monsoon season. When the Q_w was dominated by monsoonal rainfall (the R-type waters), riverine δ^7Li decreased about 1.9‰ and Li flux increased 223.7 mg/day in average, owing to short rock–fluid interaction time by rapid water flow as a strong kinetic control of silicate weathering. In relatively less rain periods during the monsoon season and the post-monsoon season, groundwater and/or landslide seepage delivered to the river channel, with relatively longer water residence times, resulted in δ^7Li increased 1.6‰ but Li flux decreased 99.4 mg/day in average compared to their neighbors, as the G-type waters. This study highlights that both monsoon climate and hydrology could have impact on the riverine Li isotope behavior. Such impacts of hydrology on riverine δ^7Li may provide some clues for the relation between Li isotopes and hydrological conditions as proposed previously (Misra and Froelich, 2012; Dellinger et al., 2015).

DATA AVAILABILITY STATEMENT

The original contributions presented in the study are included in the article/Supplementary Material, further inquiries can be directed to the corresponding author.

AUTHOR CONTRIBUTIONS

ZJ contributed to conception and designed the study. BL-L, L-FG, and YX contributed to fieldwork and guided on research methods and calculations. M-YH and FZ provided research ideas and suggestions. BL-L did the experimental work and drafted the initial manuscript with help from all authors. All authors commented on the manuscript and approved the submitted version.

FUNDING

This work was financially supported by the second Tibetan Plateau Scientific Expedition and Research (2019QZKK0707) and the NSFC grants (41991322 and 41930864).

ACKNOWLEDGMENTS

We thank Gaojun Li at Nanjing University for providing the landslide seepage data. We are grateful to Chao Zhu at Guilin University of Technology, Yulong Li at Qinghai Institute of Salt Lakes, Chinese Academy of Sciences, Chunyao Liu at University College London, and Ningpan Chai at Institute of Earth Environment, Chinese Academy of Sciences for their kind help on graphing and laboratory work.

REFERENCES

Bagard, M.-L., West, A. J., Newman, K., and Basu, A. R. (2015). Lithium Isotope Fractionation in the Ganges-Brahmaputra Floodplain and Implications for Groundwater Impact on Seawater Isotopic Composition. *Earth Planet. Sci. Lett.* 432, 404–414. doi:10.1016/j.epsl.2015.08.036

Beck, A. J., Charette, M. A., Cochran, J. K., Gonneea, M. E., and Peucker-Ehrenbrink, B. (2013). Dissolved Strontium in the Subterranean Estuary-Implications for the marine Strontium Isotope Budget. *Geochim. Cosmochim. Atca.* 117, 33–52. doi:10.1016/j.gca.2013.03.021

Bickle, M. J., Chapman, H. J., Bunbury, J., Harris, N. B. W., Fairchild, I. J., Ahmad, T., et al. (2005). Relative Contributions of Silicate and Carbonate Rocks to Riverine Sr Fluxes in the Headwaters of the Ganges. *Geochim. Cosmochim. Atca.* 69, 2221–2240. doi:10.1016/j.gca.2004.11.019

Bickle, M. J., Tipper, E., Galy, A., Chapman, H., and Harris, N. (2015). On Discrimination between Carbonate and Silicate Inputs to Himalayan Rivers. *Am. J. Sci.* 315, 120–166. doi:10.2475/02.2015.02

Bureau of Hydrology (2010). *Hydrological Data of Changjiang River Basin*. Beijing: Annual Hydrological Report.

Caves, J. K., Jost, A. B., Lau, K. V., and Maher, K. (2016). Cenozoic Carbon Cycle Imbalances and a Variable Weathering Feedback. *Earth Planet. Sci. Lett.* 450, 152–163. doi:10.1016/j.epsl.2016.06.035

Chetelat, B., Liu, C.-Q., Zhao, Z. Q., Wang, Q. L., Li, S. L., Li, J., et al. (2008). Geochemistry of the Dissolved Load of the Changjiang Basin Rivers: Anthropogenic Impacts and Chemical Weathering. *Geochim. Cosmochim. Atca.* 72, 4254–4277. doi:10.1016/j.gca.2008.06.013

Clift, P. D., Hodges, K. V., Heslop, D., Hannigan, R., Van Long, H., and Calves, G. (2008). Correlation of Himalayan Exhumation Rates and Asian Monsoon Intensity. *Nat. Geosci.* 1, 875–880. doi:10.1038/ngeo351

Dellinger, M., Gaillardet, J., Bouchez, J., Calmels, D., Galy, V., Hilton, R. G., et al. (2014). Lithium Isotopes in Large Rivers Reveal the Cannibalistic Nature of Modern Continental Weathering and Erosion. *Earth Planet. Sci. Lett.* 401, 359–372. doi:10.1016/j.epsl.2014.05.061

Dellinger, M., Gaillardet, J., Bouchez, J., Calmels, D., Louvat, P., Dosseto, A., et al. (2015). Riverine Li Isotope Fractionation in the Amazon River Basin Controlled

by the Weathering Regimes. *Geochim. Cosmochim. Atca.* 164, 71–93. doi:10.1016/j.gca.2015.04.042

Edmond, J. M. (1992). Himalayan Tectonics, Weathering Processes, and the Strontium Isotope Record in Marine Limestones. *Science* 258, 1594–1597. doi:10.2307/288205610.1126/science.258.5088.1594

Edmond, J. M., Palmer, M. R., Measures, C. I., Grant, B., and Stallard, R. F. (1995). The Fluvial Geochemistry and Denudation Rate of the Guayana Shield in Venezuela, Colombia, and Brazil. *Geochim. Cosmochim. Atca.* 59 (16), 3301–3325. doi:10.1016/0016-7037(95)00128-m

Fries, D. M., James, R. H., Dessert, C., Bouchez, J., Beaumais, A., and Pearce, C. R. (2019). The Response of Li and Mg Isotopes to Rain Events in a Highly-Weathered Catchment. *Chem. Geol.*. 519, 68–82. doi:10.1016/j.chemgeo.2019.04.023

Gaillardet, J., Dupre, B., Allegre, C. J., and Négrel, P. (1997). Chemical and Physical Denudation in the Amazon River Basin. *Chem. Geol.* 142 (3–4), 141–173. doi:10.1016/s0009-2541(97)00074-0

Gaillardet, J., Dupré, B., Louvat, P., and Allègre, C. J. (1999). Global Silicate Weathering and CO_2 Consumption Rates Deduced from the Chemistry of Large Rivers. *Chem. Geol.* 159 (1–4), 3–30. doi:10.1016/s0009-2541(99)00031-5

Galy, A., and France-Lanord, C. (1999). Weathering Processes in the Ganges–Brahmaputra Basin and the Riverine Alkalinity Budget. *Chem. Geol.* 159 (1–4), 31–60. doi:10.1016/s0009-2541(99)00033-9

Gou, L.-F., Jin, Z., Deng, L., He, M.-Y., and Liu, C.-Y. (2018). Effects of Different Cone Combinations on Accurate and Precise Determination of Li Isotopic Composition by MC-ICP-MS. *Spectrochimica Acta B: At. Spectrosc.* 146, 1–8. doi:10.1016/j.sab.2018.04.015

Gou, L.-F., Jin, Z., Deng, L., Sun, H., Yu, H. M., and Zhang, F. (2017). Efficient Purification for Li and High-Precision and Accuracy Determination of Li Isotopic Composition by MC-ICP-MS. *Geochimica* 46 (6), 528–537 [In Chinese With English Abstract]. doi:10.3969/j.issn.0379-1726.2017.06.003

Gou, L.-F., Jin, Z., Pogge von Strandmann, P. A. E., Li, G., Qu, Y.-X., Xiao, J., et al. (2019). Li Isotopes in the Middle Yellow River: Seasonal Variability, Sources and Fractionation. *Geochim. Cosmochim. Atca.* 248, 88–108. doi:10.1016/j.gca.2019.01.007

Gou, L.-F., Liu, C. Y., Deng, L., and Jin, Z. (2020). Quantifying the Impact of Recovery during Chromatographic Purification on the Accuracy of Lithium Isotopic Determination by Multi-Collector Inductively Coupled Plasma Mass Spectrometry. *Rapid Commun. Mass. Spectrom.* 34, e8577. doi:10.1002/rcm.8577

Hagedorn, B., and Cartwright, I. (2009). Climatic and Lithologic Controls on the Temporal and Spatial Variability of CO_2 Consumption via Chemical Weathering: An Example from the Australian Victorian Alps. *Chem. Geol.*. 260, 234–253. doi:10.1016/j.chemgeo.2008.12.019

Hathorne, E., and James, R. (2006). Temporal Record of Lithium in Seawater: A Tracer for Silicate Weathering? *Earth Planet. Sci. Lett.* 246 (3–4), 393–406. doi:10.1016/j.epsl.2006.04.020

Hu, W., and Zhou, Q. (2012). Characteristics and Applications of Lithium Isotope Geochemistry. *Sci. Tech. Inform.* (5), 244 [In Chinese With English Abstract].

Huh, Y., Chan, L.-H., and Edmond, J. M. (2001). Lithium Isotopes as a Probe of Weathering Processes: Orinoco River. *Earth Planet. Sci. Lett.* 194 (1–2), 189–199. doi:10.1016/s0012-821x(01)00523-4

Huh, Y., Chan, L.-H., Zhang, L., and Edmond, J. M. (1998). Lithium and its Isotopes in Major World Rivers: Implications for Weathering and the Oceanic Budget. *Geochim. Cosmochim. Atca.* 62 (12), 2039–2051. doi:10.1016/s0016-7037(98)00126-4

Jin, Z., West, A. J., Zhang, F., An, Z., Hilton, R. G., Yu, J., et al. (2016). Seismically Enhanced Solute Fluxes in the Yangtze River Headwaters Following the A.D. 2008 Wenchuan Earthquake. *Geology* 44 (1), 47–50. doi:10.1130/g37246.1

Kısakűrek, B., James, R. H., and Harris, N. B. W. (2005). Li and δ^7Li in Himalayan Rivers: Proxies for Silicate Weathering? *Earth Planet. Sci. Lett.* 237, 387–401. doi:10.1016/j.epsl.2005.07.019

Kloppmann, W., Négrel, P., Casanova, J., Klinge, H., Schelkes, K., and Guerrot, C. (2001). Halite Dissolution Derived Brines in the Vicinity of a Permian Salt Dome (N German Basin). Evidence from Boron, Strontium, Oxygen, and Hydrogen Isotopes. *Geochim. Cosmochim. Atca.* 65 (22), 4087–4101. doi:10.1016/s0016-7037(01)00640-8

Koger, J. M., Newman, B. D., and Goering, T. J. (2018). Chemostatic Behaviour of Major Ions and Contaminants in a Semiarid Spring and Stream System Near Los Alamos, NM, USA. *Hydrological Process.* 32 (11), 1709–1716. doi:10.1002/hyp.11624

Lemarchand, E., Chabaux, F., Vigier, N., Millot, R., and Pierret, M.-C. (2010). Lithium Isotope Systematics in a Forested Granitic Catchment (Strengbach, Vosges Mountains, France). *Geochim. Cosmochim. Atca.* 74 (16), 4612–4628. doi:10.1016/j.gca.2010.04.057

Li, G., West, A. J., Densmore, A. L., Jin, Z., Parker, R. N., and Hilton, R. G. (2014). Seismic Mountain Building: Landslides Associated with the 2008 Wenchuan Earthquake in the Context of a Generalized Model for Earthquake Volume Balance. *Geochem. Geophys. Geosyst.* 15, 833–844. doi:10.1002/2013GC005067

Li, J., and Zhang, J. (2002). Weathering of Watershed Basins and Global Climate Change. *Adv. Earth Sci.* 17 (3), 411–419 [In Chinese With English Abstract]. doi:10.11867/j.issn.1001-8166.2002.03.0411

Li, S.-L., Chetelat, B., Yue, F., Zhao, Z., and Liu, C.-Q. (2014). Chemical Weathering Processes in the Yalong River Draining the Eastern Tibetan Plateau, China. *J. Asian Earth Sci.* 88, 74–84. doi:10.1016/j.jseaes.2014.03.011

Liu, F., Yin, X., and Liu, Q. (2021). Lithium Isotopes and Continental Weathering. *Acta Mineral. Sinica* 41 (2), 127–138 [In Chinese With English Abstract]. doi:10.16461/j.cnki.1000-4734.2021.41.054

Liu, M., Zhao, L. Y., Li, Q. Y., Zou, J. Y., Hu, Y., Zhang, Y. Z., et al. (2021). Hydrological Characteristics, Main Ion Sources of Main Rivers in the Souce Region of Yangtze River. *China Envion. Sci.* 41 (3), 1243–1254 [In Chinese With English Abstract]. doi:10.3969/j.issn.1000-6923.2021.03.028

Liu, X.-M., Fu, Y.-H., and Xia, R-J. (2020). Opportunities and Challenges of Watershed Ecological Comprehensive Conpensation–Taking the Min Jiang River Basin in Sichuan Province as an Example. *Environ. Ecol.* 2 (9), 25–30 [In Chinese With English Abstract].

Liu, X.-M., and Rudnick, R. L. (2011). Constraints on Continental Crustal Mass Loss via Chemical Weathering Using Lithium and its Isotopes. *Proc. Natl. Acad. Sci. U.S.A.* 108 (52), 20873–20880. doi:10.1073/pnas.1115671108

Liu, X.-M., Wanner, C., Rudnick, R. L., and McDonough, W. F. (2015). Processes Controlling δ^7Li in Rivers Illuminated by Study of Streams and Groundwaters Draining Basalts. *Earth Planet. Sci. Lett.* 409, 212–224. doi:10.1016/j.epsl.2014.10.032

Luijendijk, E., Gleeson, T., and Moosdorf, N. (2020). Fresh Groundwater Discharge Insignificant for the World's Oceans but Important for Coastal Ecosystems. *Nat. Commun.* 11, 1–12. doi:10.1038/s41467-020-15064-8

Ma, T., Weynell, M., Li, S.-L., Liu, Y., Chetelat, B., Zhong, J., et al. (2020). Lithium Isotope Compositions of the Yangtze River Headwaters: Weathering in High-Relief Catchments. *Geochim. Cosmochim. Atca.* 280, 46–65. doi:10.1016/j.gca.2020.03.029

Maher, K., and Chamberlain, C. P. (2014). Hydrologic Regulation of Chemical Weathering and the Geologic Carbon Cycle. *Science* 343 (6178), 1502–1504. doi:10.1126/science.1250770

Manaka, T., Araoka, D., Yoshimura, T., Hossain, H. M. Z., Nishio, Y., Suzuki, A., et al. (2017). Downstream and Seasonal Changes of Lithium Isotope Ratios in the Ganges-Brahmaputra River System. *Geochem. Geophys. Geosyst.* 18, 3003–3015. doi:10.1002/2016gc006738

Mavromatis, V., Rinder, T., Prokushkin, A. S., Pokrovsky, O. S., Korets, M. A., Chmeleff, J., et al. (2016). The Effect of Permafrost, Vegetation, and Lithology on Mg and Si Isotope Composition of the Yenisey River and its Tributaries at the End of the Spring Flood. *Geochim. Cosmochim. Atca.* 191, 32–46. doi:10.1016/j.gca.2016.07.003

Mayfield, K. K., Eisenhauer, A., Santiago Ramos, D. P., Higgins, J. A., Horner, T. J., Auro, M., et al. (2021). Groundwater Discharge Impacts Marine Isotope Budgets of Li, Mg, Ca, Sr, and Ba. *Nat. Commun.* 12 (1), 1–9. doi:10.1038/s41467-020-20248-3

Meybeck, M. (1987). Global Chemical Weathering of Surficial Rocks Estimated from River Dissolved Loads. *Am. J. Sci.* 287 (5), 401–428. doi:10.2475/ajs.287.5.401

Millot, R., Gaillardet, J. é., Dupré, B., and Allègre, C. J. (2003). Northern Latitude Chemical Weathering Rates: Clues from the Mackenzie River Basin, Canada. *Geochim. Cosmochim. Atca.* 67 (7), 1305–1329. doi:10.1016/S0016-7037(02)01207-3

Millot, R., Petelet-Giraud, E., Guerrot, C., and Négrel, P. (2010a). Multi-isotopic Composition (δ^7Li-Δ^{11}b-Δd-Δ^{18}o) of Rainwaters in France: Origin and Spatio-Temporal Characterization. *Appl. Geochem.* 25 (10), 1510–1524. doi:10.1016/j.apgeochem.2010.08.002

Millot, R., Vigier, N., and Gaillardet, J. (2010b). Behaviour of Lithium and its Isotopes during Weathering in the Mackenzie Basin, Canada. *Geochim. Cosmochim. Atca.* 74 (14), 3897–3912. doi:10.1016/j.gca.2010.04.025

Misra, S., and Froelich, P. N. (2012). Lithium Isotope History of Cenozoic Seawater: Changes in Silicate Weathering and Reverse Weathering. *Science* 335, 818–823. doi:10.1126/science.1214697

Moquet, J.-S., Crave, A., Viers, J., Seyler, P., Armijos, E., Bourrel, L., et al. (2011). Chemical Weathering and Atmospheric/soil CO_2 Uptake in the Andean and Foreland Amazon Basins. *Chem. Geol.*. 287, 1–26. doi:10.1016/j.chemgeo.2011.01.005

Penman, D. E., Caves Rugenstein, J. K., Ibarra, D. E., and Winnick, M. J. (2020). Silicate Weathering as a Feedback and Forcing in Earth's Climate and Carbon Cycle. *Earth-Sci. Rev.* 209, 103298. doi:10.1016/j.earscirev.2020.103298

Pogge von Strandmann, P. A. E., Burton, K. W., James, R. H., van Calsteren, P., Gíslason, S. R., and Mokadem, F. (2006). Riverine Behaviour of Uranium and Lithium Isotopes in an Actively Glaciated Basaltic Terrain. *Earth Planet. Sci. Lett.* 251 (1–2), 134–147. doi:10.1016/j.epsl.2006.09.001

Pogge von Strandmann, P. A. E., Burton, K. W., Opfergelt, S., Eiríksdóttir, E. S., Murphy, M. J., Einarsson, A., et al. (2016). The Effect of Hydrothermal Spring Weathering Processes and Primary Productivity on Lithium Isotopes: Lake Myvatn, Iceland. *Chem. Geology*. 445, 4–13. doi:10.1016/j.chemgeo.2016.02.026

Pogge von Strandmann, P. A. E., Fraser, W. T., Hammond, S. J., Tarbuck, G., Wood, I. G., Oelkers, E. H., et al. (2019). Experimental Determination of Li Isotope Behaviour during Basalt Weathering. *Chem. Geol.*. 517, 34–43. doi:10.1016/j.chemgeo.2019.04.020

Pogge von Strandmann, P. A. E., Frings, P. J., and Murphy, M. J. (2017). Lithium Isotope Behaviour during Weathering in the Ganges Alluvial Plain. *Geochim. Cosmochim. Atca.* 198, 17–31. doi:10.1016/j.gca.2016.11.017

Pogge von Strandmann, P. A. E., Jenkyns, H. C., and Woodfine, R. G. (2013). Lithium Isotope Evidence for Enhanced Weathering during Oceanic Anoxic Event 2. *Nat. Geosci.* 6 (8), 668–672. doi:10.1038/ngeo1875

Qin, J., Huh, Y., Edmond, J. M., Du, G., and Ran, J. (2006). Chemical and Physical Weathering in the Min Jiang, a Headwater Tributary of the Yangtze River. *Chem. Geol.*. 227 (1–2), 53–69. doi:10.1016/j.chemgeo.2005.09.011

Qin, J., Pan, G., and Du, G. (2000). The Effects of Cenozoic Tectonic Uplift on Earth Surface Chemical Weathering and Global Climate Change. *Earth Sci. Front.* 7 (2), 517–525. doi:10.3321/j.issn:1005-2321.2000.02.019

Ravizza, G., and Esser, B. K. (1993). A Possible Link between the Seawater Osmium Isotope Record and Weathering of Ancient Sedimentary Organic Matter. *Chem. Geol.* 107 (3–4), 255–258. doi:10.1016/0009-2541(93)90186-m

Raymo, M. E., and Ruddiman, W. F. (1992). Tectonic Forcing of Late Cenozoic Climate. *Nature* 359 (6391), 117–122. doi:10.1038/359117a0

Rudnick, R. L., Tomascak, P. B., Njo, H. B., and Gardner, L. R. (2004). Extreme Lithium Isotopic Fractionation during Continental Weathering Revealed in Saprolites from South Carolina. *Chem. Geol.*. 212 (1–2), 45–57. doi:10.1016/j.chemgeo.2004.08.008

SLCCC (Sichuan Local Chronicles Compilation Committee) (1998). *Commision on Annals of Sichuan Province (1998)*. Chengdu: Science and Technological Publishing House of Sichuan Province.

Su, Y. (2012). *Research Progress of Lithium Isotope in Underground waterNational Conference of Water Resource Allocation and Optimal Scheduling Technique*. China: Xi'an.

Tipper, E. T., Bickle, M. J., Galy, A., West, A. J., Pomiès, C., and Chapman, H. J. (2006). The Short Term Climatic Sensitivity of Carbonate and Silicate Weathering Fluxes: Insight from Seasonal Variations in River Chemistry. *Geochim. Cosmochim. Atca.* 70, 2737–2754. doi:10.1016/j.gca.2006.03.005

Vigier, N., Decarreau, A., Millot, R., Carignan, J., Petit, S., and France-Lanord, C. (2008). Quantifying Li Isotope Fractionation during Smectite Formation and Implications for the Li Cycle. *Geochim. Cosmochim. Atca.* 72 (3), 780–792. doi:10.1016/j.gca.2007.11.011

Vigier, N., Gislason, S. R., Burton, K. W., Millot, R., and Mokadem, F. (2009). The Relationship between Riverine Lithium Isotope Composition and Silicate Weathering Rates in Iceland. *Earth Planet. Sci. Lett.* 287, 434–441. doi:10.1016/j.epsl.2009.08.026

Walker, J. C. G., Hays, P. B., and Kasting, J. F. (1981). A Negative Feedback Mechanism for the Long-Term Stabilization of Earth's Surface Temperature. *J. Geophys. Res.* 86 (C10), 9776. doi:10.1029/jc086ic10p09776

Wang, J., Jin, Z., Hilton, R. G., Zhang, F., Densmore, A. L., Li, G., et al. (2015). Controls on Fluvial Evacuation of Sediment from Earthquake-Triggered Landslides. *Geology* 43, 115–118. doi:10.1130/G36157.1

Wang, Q.-L., Chetelat, B., Zhao, Z.-Q., Ding, H., Li, S.-L., Wang, B.-L., et al. (2015). Behavior of Lithium Isotopes in the Changjiang River System: Sources Effects and Response to Weathering and Erosion. *Geochim. Cosmochim. Atca.* 151, 117–132. doi:10.1016/j.gca.2014.12.015

West, A. J., Bickle, M. J., Collins, R., and Brasington, J. (2002). Small-catchment Perspective on Himalayan Weathering Fluxes. *Geology* 30 (4), 355. doi:10.1130/0091-7613(2002)030<0355:SCPOHW>2.0.CO;2

Wu, L., Huh, Y., Qin, J., Du, G., and van Der Lee, S. (2005). Chemical Weathering in the Upper Huang He (Yellow River) Draining the Eastern Qinghai-Tibet Plateau. *Geochim. Cosmochim. Atca.* 69 (22), 5279–5294. doi:10.1016/j.gca.2005.07.001

Wu, W., Xu, S., Yang, J., and Yin, H. (2008). Silicate Weathering and CO_2 Consumption Deduced from the Seven Chinese Rivers Originating in the Qinghai-Tibet Plateau. *Chem. Geol.*. 249, 307–320. doi:10.1016/j.chemgeo.2008.01.025

Wu, W., Zheng, H., Yang, J., Chao, L., and Zhou, B. (2011). Chemical Weathering of Larger River Catchments in China and the Global Carbon Cycle. *Quat. Sci.* 31 (3), 397–407 [In Chinese With English Abstract]. doi:10.3969/j.issn.1001-7410.2011.03.01

Xu, Z., Li, T., Li, G., Hedding, D. W., Wang, Y., Gou, L.-F., et al. (2021). Lithium Isotopic Composition of Soil Pore Water: Responses to Evapotranspiration. *Geology* 50, 194–198. doi:10.1130/G49366.1

Yoon, J., Huh, Y., Lee, I., Moon, S., Noh, H., and Qin, J. (2008). Weathering Processes in the Min Jiang: Major Elements, $^{87}Sr/^{86}Sr$, $\delta^{34}S_{SO4}$, and $\delta^{18}O_{SO4}$. *Aquat. Geochem.* 14, 147–170. doi:10.1007/s10498-008-9030-7

Zhang, H., Yang, N., Zhang, Y., and Meng, H. (2006). Geomorphology of the Minjiang Drainage System (Sichuan, China) and its Structural Implications. *Quat. Sci.* 26 (1), 126–135. doi:10.3321/j.issn:1001-7410.2006.01.016

Zhang, Q., Jin, Z., Zhang, F., and Xiao, J. (2015). Seasonal Variation in River Water Chemistry of the Middle Reaches of the Yellow River and its Controlling Factors. *J. Geochem. Explor.* 156, 101–113. doi:10.1016/j.gexplo.2015.05.008

Conflict of Interest: The authors declare that the research was conducted in the absence of any commercial or financial relationships that could be construed as a potential conflict of interest.

Publisher's Note: All claims expressed in this article are solely those of the authors and do not necessarily represent those of their affiliated organizations, or those of the publisher, the editors, and the reviewers. Any product that may be evaluated in this article, or claim that may be made by its manufacturer, is not guaranteed or endorsed by the publisher.